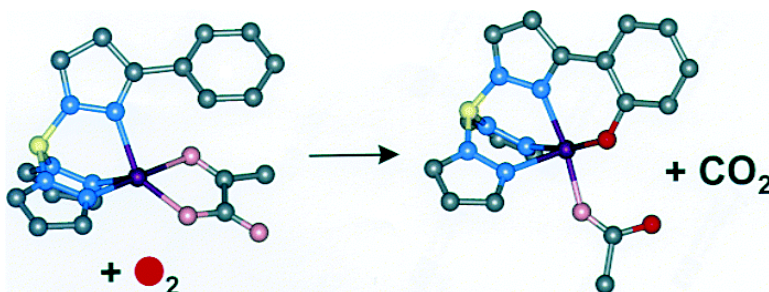


Oxygen Activation by Nonheme Iron(II) Complexes: β -Keto Carboxylate versus Carboxylate

Mark P. Mehn, Kiyoshi Fujisawa, Eric L. Hegg, and Lawrence Que

J. Am. Chem. Soc., **2003**, 125 (26), 7828-7842 • DOI: 10.1021/ja028867f • Publication Date (Web): 10 June 2003

Downloaded from <http://pubs.acs.org> on March 29, 2009



More About This Article

Additional resources and features associated with this article are available within the HTML version:

- Supporting Information
- Links to the 7 articles that cite this article, as of the time of this article download
- Access to high resolution figures
- Links to articles and content related to this article
- Copyright permission to reproduce figures and/or text from this article

[View the Full Text HTML](#)

Oxygen Activation by Nonheme Iron(II) Complexes: α -Keto Carboxylate versus Carboxylate

Mark P. Mehn,[†] Kiyoshi Fujisawa,^{*,‡} Eric L. Hegg,^{†,§} and Lawrence Que, Jr.^{*,†}

Contribution from the Department of Chemistry and Center for Metals in Biocatalysis, 207 Pleasant Street Southeast, University of Minnesota, Minneapolis, Minnesota 55455, and Department of Chemistry, University of Tsukuba, Tennodai 1-1-1, Tsukuba 305-8571, Japan

Received October 8, 2002; E-mail: kiyoshif@chem.tsukuba.ac.jp; que@chem.umn.edu

Abstract: Mononuclear iron(II) α -keto carboxylate and carboxylate compounds of the sterically hindered tridentate face-capping ligand Tp^{Ph_2} (Tp^{Ph_2} = hydrotris(3,5-diphenylpyrazol-1-yl)borate) were prepared as models for the active sites of nonheme iron oxygenases. The structures of an aliphatic α -keto carboxylate complex, $[\text{Fe}^{\text{II}}(\text{Tp}^{\text{Ph}_2})(\text{O}_2\text{CC}(\text{O})\text{CH}_3)]$, and the carboxylate complexes $[\text{Fe}^{\text{II}}(\text{Tp}^{\text{Ph}_2})(\text{OBz})]$ and $[\text{Fe}^{\text{II}}(\text{Tp}^{\text{Ph}_2})(\text{OAc})(3,5\text{-Ph}_2\text{pzH})]$ were determined by single-crystal X-ray diffraction, all of which have five-coordinate iron centers. Both the α -keto carboxylate and the carboxylate compounds react with dioxygen resulting in the hydroxylation of a single ortho phenyl position of the Tp^{Ph_2} ligand. The oxygenation products were characterized spectroscopically, and the structure of the octahedral iron(III) phenolate product $[\text{Fe}^{\text{III}}(\text{Tp}^{\text{Ph}_2})(\text{OAc})(3,5\text{-Ph}_2\text{pzH})]$ was established by X-ray diffraction. The reaction of the α -keto carboxylate model compounds with oxygen to produce the phenolate product occurs with concomitant oxidative decarboxylation of the α -keto acid. Isotope labeling studies show that $^{18}\text{O}_2$ ends up in the Tp^{Ph_2} phenolate oxygen and the carboxylate derived from the α -keto acid. The isotope incorporation mirrors the dioxygenase nature of the enzymatic systems. Parallel studies on the carboxylate complexes demonstrate that the oxygen in the hydroxylated ligand is also derived from molecular oxygen. The oxygenation of the benzoylformate complex is demonstrated to be first order in metal complex and dioxygen, with activation parameters $\Delta H^\ddagger = 25 \pm 2 \text{ kJ mol}^{-1}$ and $\Delta S^\ddagger = -179 \pm 6 \text{ J mol}^{-1} \text{ K}^{-1}$. The rate of appearance of the iron(III) phenolate product is sensitive to the nature of the substituent on the benzoylformate ligand, exhibiting a Hammett ρ value of $+1.3$ indicative of a nucleophilic mechanism. The proposed reaction mechanism involves dioxygen binding to produce an iron(III) superoxide species, nucleophilic attack of the superoxide at the α -keto functionality, and oxidative decarboxylation of the adduct to afford the oxidizing species that attacks the Tp^{Ph_2} phenyl ring. Interestingly, the α -keto carboxylate complexes react 2 orders of magnitude faster than the carboxylate complexes, thus emphasizing the key role that the α -keto functionality plays in oxygen activation by α -keto acid-dependent iron enzymes.

α -Ketoglutarate (α -KG)¹-dependent dioxygenases constitute a large class of nonheme iron-containing enzymes that are essential for the biosynthesis of a diverse array of compounds,² catabolism of selected biomolecules,³ repair of alkylated DNA^{4,5} and RNA,⁶ and oxygen sensing in cells.⁷⁻⁹ For instance, prolyl hydroxylase is responsible for the posttranslational modification of proline to hydroxyproline in collagen biosynthesis¹⁰ and in

the cellular response to hypoxia,⁷⁻⁹ clavaminic acid synthase (CAS) catalyzes three distinct steps in the synthesis of the β -lactamase inhibitor clavulanic acid,¹¹ AlkB demethylates 1-methyladenine and 3-methylcytosine in single stranded DNA and RNA,⁴⁻⁶ and deacetoxycephalosporin C synthase (DAOCS) catalyzes the ring expansion of the thiazolidine ring of the penicillin N nucleus to afford deacetoxycephalosporin C (Scheme 1).^{12,13} Although each enzyme carries out a distinct transformation, the members of this class share a requirement for an α -keto

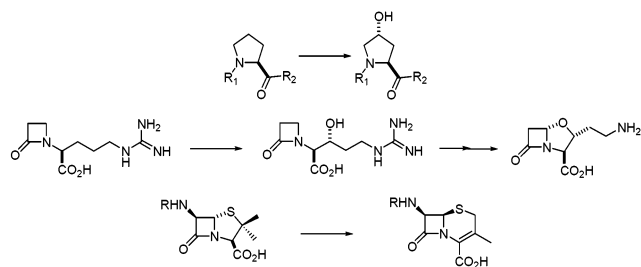
[†] University of Minnesota.

[‡] University of Tsukuba.

[§] Current address: Department of Chemistry, University of Utah, Salt Lake City, UT 84112.

- (1) Abbreviations: α -KG, α -ketoglutarate; BF, benzoylformate; CAS, clavaminic synthase 2; DAOCS, deacetoxycephalosporin C synthase; 3,5-Ph₂pzH, 3,5-diphenylpyrazole; 6-Me₃-TPA, tris(6-methyl-2-pyridylmethyl)amine; PRV, pyruvate; TfdA, 2,4-dichlorophenoxyacetic acid/ α -KG dioxygenase; TauD, taurine/ α -KG dioxygenase; TPA, tris(2-pyridylmethyl)amine; $\text{Tp}^{\text{Bu}_2\text{Pr}}$, hydrotris(3-*tert*-butyl-5-isopropylpyrazol-1-yl)borate (monoanion); Tp^{Pr_2} , hydrotris(3,5-diisopropylpyrazol-1-yl)borate (monoanion); Tp^{Me_2} , hydrotris(3,5-dimethylpyrazol-1-yl)borate (monoanion); Tp^{Ph_2} , hydrotris(3,5-diphenylpyrazol-1-yl)borate (monoanion).
- (2) Prescott, A. G.; Lloyd, M. D. *Nat. Prod. Rep.* **2000**, *17*, 367–383.
- (3) De Carolis, E.; De Luca, V. *Phytochemistry* **1994**, *36*, 1093–1107.
- (4) Falnes, P. Ø.; Johansen, R. F.; Seeberg, E. *Nature* **2002**, *419*, 178–182.
- (5) Trewick, S. C.; Henshaw, T. F.; Hausinger, R. P.; Lindahl, T.; Sedgwick, B. *Nature* **2002**, *419*, 174–178.

- (6) Aas, P. A.; Otterlei, M.; Falnes, P. Ø.; Vågbo, C. B.; Skorpén, F.; Akbari, M.; Sundheim, O.; Björås, M.; Slupphaug, G.; Seeberg, E.; Krokan, H. E. *Nature* **2003**, *421*, 859–863.
- (7) Ivan, M.; Kondo, K.; Yang, H.; Valiando, J.; Ohh, M.; Salic, A.; Asara, J. M.; Lane, W. S.; Kaelin, W. G., Jr. *Science* **2001**, *292*, 464–468.
- (8) Jaakkola, P.; Mole, D. R.; Tian, Y.-M.; Wilson, M. I.; Gielbert, J.; Gaskell, S. J.; von Kriegsheim, A.; Hebestreit, H. F.; Mukherji, M.; Schofield, C. J.; Maxwell, P. H.; Pugh, C. W.; Ratcliffe, P. J. *Science* **2001**, *292*, 468–472.
- (9) Lando, D.; Peet, D. J.; Whelan, D. A.; Gorman, J. J.; Whitelaw, M. L. *Science* **2002**, *295*, 858–861.
- (10) Kivirikko, K. I.; Myllylä, R.; Pihlajaniemi, T. *FASEB J.* **1989**, *3*, 1609–1617.
- (11) Salowe, S. P.; Marsh, E. N.; Townsend, C. A. *Biochemistry* **1990**, *29*, 6499–6508.

Scheme 1. Reactions Catalyzed by α -Keto Carboxylate-Dependent Oxygenases^a

^a Prolyl hydroxylase (top), CAS (middle), and DAOCs (bottom).

acid, dioxygen, and iron(II). The iron(II) is bound to a common 2-His-1-carboxylate facial triad,¹⁴ which to date has been observed crystallographically for several enzymes in this subclass, including DAOCs,¹⁵ *p*-hydroxyphenylpyruvate dioxygenase,¹⁶ CAS,¹⁷ prolyl hydroxylase,¹⁸ anthocyanidin synthase,¹⁹ and taurine/ α -ketoglutarate dioxygenase (TauD).²⁰ The remaining coordination sites are occupied by water molecules that can be displaced by exogenous ligands such as the α -keto acid, NO, and presumably O₂.^{15,17,19–21}

A common mechanism has been proposed for these enzymes (Scheme 2).^{22–24} In the first step, the α -keto acid chelates to the iron(II) center, displacing two solvent molecules. Substrate binding in the vicinity of the iron active site then results in the displacement of the remaining water ligand, generating a coordinatively unsaturated metal center ready to bind and activate dioxygen.^{22–25} O₂ binds to the iron(II) center and attacks the keto carbon of the α -keto acid generating an iron(IV)-peroxo intermediate that then undergoes O–O bond cleavage and decarboxylation to afford an iron(IV)-oxo oxidant. After substrate oxidation, the product, succinate, and CO₂ dissociate from the active site to complete the catalytic cycle. Crystal structures of enzyme- α -KG, enzyme- α -KG-substrate, and enzyme-succinate-CO₂ complexes support this scheme.^{15,17–20,26}

While the enzymatic studies provide a firm foundation for the steps leading to and from substrate oxidation, deeper insight into the mechanism of the metal-centered oxidation is desirable. Toward this goal, several complexes have been synthesized as models that provide a basis for understanding oxygen activation by α -keto acid-dependent enzymes;^{27–31} yet only for one, [Fe-

(Tp^{Ph2})(BF)], has the dioxygenase activity observed in α -keto acid-dependent enzymes been demonstrated.³⁰ In this case, the oxidative decarboxylation of benzoylformate (BF) results in the incorporation of one atom of dioxygen into the hydroxylated phenyl ring of the ligand and the other into the benzoate byproduct of this reaction. To better understand the role of the α -keto carboxylate cofactor in oxygen activation at mononuclear nonheme iron enzymes, we have synthesized an expanded series of [Fe^{II}(Tp^{Ph2})(X)] model complexes with α -keto carboxylates and corresponding carboxylates and examined the structures and reactivity of these compounds. These studies demonstrate that the α -keto acid cofactor serves as a sacrificial two-electron reductant and facilitates production of a reactive oxygen species at the iron center that hydroxylates a phenyl ring of the Tp^{Ph2} ligand. The corresponding carboxylate model complexes also activate O₂, but the reactions proceed much more slowly. This dramatic difference emphasizes the importance of α -keto acid cofactors in promoting the activation of dioxygen at nonheme iron(II) centers in biology.

Experimental Procedures

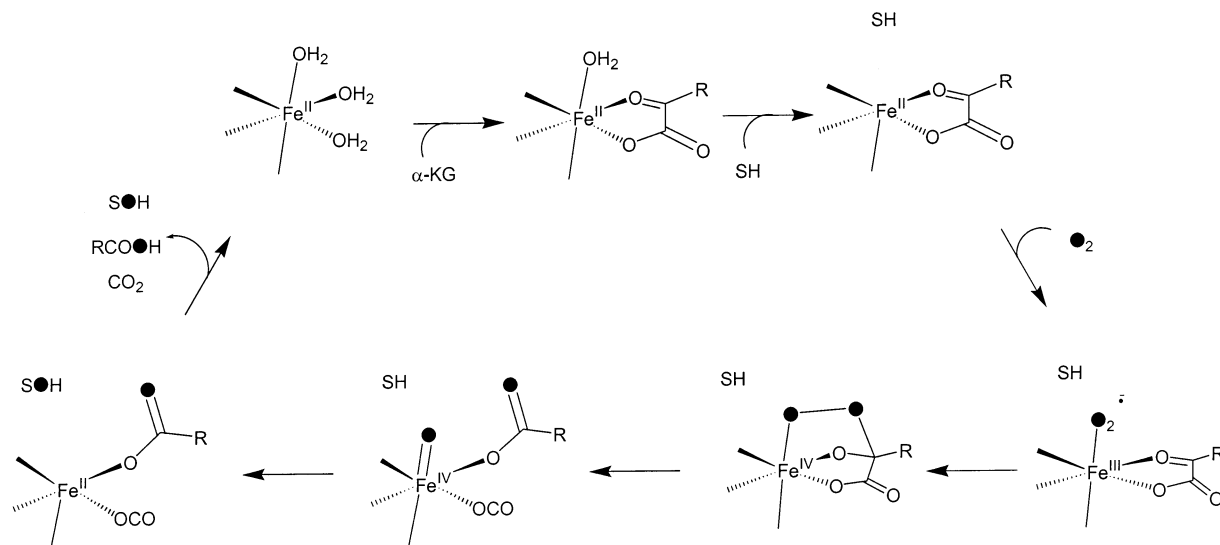
General Materials and Syntheses. All reagents and solvents were purchased from commercial sources and were used without further purification unless otherwise noted. Methanol was distilled from Mg-(OMe)₂ before use. Thiophene-free benzene was distilled from sodium/benzophenone ketyl under an argon atmosphere prior to use. Dichloromethane, acetonitrile, and *n*-heptane were carefully purified by distillation under an argon atmosphere from P₂O₅, CaH₂, and sodium/benzophenone ketyl, respectively.³² Preparation and handling of air-sensitive materials were carried out under inert atmosphere using standard Schlenk techniques or a glovebox. Caution: Although no problems were encountered with these complexes, perchlorate salts are potentially explosive and should be handled with care.

The ligand K(Tp^{Ph2}) was prepared as previously reported.³³ Benzoylformic acid and its sodium salt were purchased from Aldrich. Sodium (*p*-methoxybenzoyl)formate was prepared by Friedel–Crafts acylation of anisole with ethyl oxalyl chloride followed by hydrolysis of the resultant ester with 4 N NaOH (aq) to yield the sodium salt.³⁴ ¹H NMR (D₂O, 300 MHz) δ (ppm): 7.86 (2H, d, 8 Hz), 7.02 (2H, d, 8 Hz), 3.83 (3H, s); ¹³C NMR (D₂O, 75.5 MHz) δ (ppm): 196, 173, 164, 132, 125, 114, 55. The ethyl esters of (*p*-methylbenzoyl)formic acid, (*p*-chlorobenzoyl)formic acid, and (*p*-fluorobenzoyl)formic acid were prepared by treating ethyl α -oxo-1H-imidazole-1-acetate with the appropriate aryl Grignard reagent.³⁵ The substituted α -keto acids were obtained in 75–90% yield by base-catalyzed hydrolysis of the resulting ethyl esters with 4 N NaOH (aq) at room temperature for 4 h.²⁷ (*m*-Nitrobenzoyl)formic acid was prepared by nitration of benzoylformic acid with concentrated HNO₃/H₂SO₄ using literature procedures.^{27,34}

[Fe(Tp^{Ph2})(BF)] (1) was prepared following a modification of the published procedure.³⁶ The sodium salt of benzoylformic acid, NaBF

- (12) Baldwin, J. E.; Abraham, E. *Nat. Prod. Rep.* **1988**, *5*, 129–145.
 (13) Baldwin, J. E.; Adlington, R. M.; Crouch, N. P.; Schofield, C. J.; Turner, N. J.; Aplin, R. T. *Tetrahedron* **1991**, *47*, 9881–9900.
 (14) Hegg, E. L.; Que, L., Jr. *Eur. J. Biochem.* **1997**, *250*, 625–629.
 (15) Valegård, K.; Terwisscha van Scheltinga, A. C.; Lloyd, M. D.; Hara, T.; Ramaswamy, S.; Perrakis, A.; Thompson, A.; Lee, H.-J.; Baldwin, J. E.; Schofield, C. J.; Hajdu, J.; Andersson, I. *Nature* **1998**, *394*, 805–809.
 (16) Serre, L.; Sailland, A.; Sy, D.; Boudec, P.; Rolland, A.; Pebay-Peyroula, E.; Cohen-Addad, C. *Structure* **1999**, *7*, 977–988.
 (17) Zhang, Z.; Ren, J.; Stammers, D. K.; Baldwin, J. E.; Harlos, K.; Schofield, C. J. *Nat. Struct. Biol.* **2000**, *7*, 127–133.
 (18) Clifton, I. J.; Hsueh, L.-C.; Baldwin, J. E.; Harlos, K.; Schofield, C. J. *Eur. J. Biochem.* **2001**, *268*, 6625–6636.
 (19) Wilmoth, R. C.; Turnbull, J. J.; Welford, R. W. D.; Clifton, I. J.; Prescott, A. G.; Schofield, C. J. *Structure* **2002**, *10*, 93–103.
 (20) Elkins, J. M.; Ryle, M. J.; Clifton, I. J.; Hotopp, J. C. D.; Lloyd, J. S.; Burzlaff, N. I.; Baldwin, J. E.; Hausinger, R. P.; Roach, P. L. *Biochemistry* **2002**, *41*, 5185–5192.
 (21) Zhang, Z.; Ren, J.-s.; Harlos, K.; McKinnon, C. H.; Clifton, I. J.; Schofield, C. J. *FEBS Lett.* **2002**, *517*, 7–12.
 (22) Hanauke-Abel, H. M.; Günzler, V. *J. Theor. Biol.* **1982**, *94*, 421–455.
 (23) Que, L., Jr.; Ho, R. Y. N. *Chem. Rev.* **1996**, *96*, 2607–2624.
 (24) Solomon, E. I.; Brunold, T. C.; Davis, M. I.; Kemsley, J. N.; Lee, S.-K.; Lehnert, N.; Neese, F.; Skulan, A. J.; Yang, Y.-S.; Zhou, J. *Chem. Rev.* **2000**, *100*, 235–349.
 (25) Schofield, C. J.; Zhang, Z. *Curr. Opin. Struct. Biol.* **1999**, *9*, 722–731.
 (26) Lee, H.-J.; Lloyd, M. D.; Harlos, K.; Clifton, I. J.; Baldwin, J. E.; Schofield, C. J. *J. Mol. Biol.* **2001**, *308*, 937–948.

- (27) Chiou, Y.-M.; Que, L., Jr. *J. Am. Chem. Soc.* **1995**, *117*, 3999–4013.
 (28) Ha, E. H.; Ho, R. Y. N.; Kisiel, J. F.; Valentine, J. S. *Inorg. Chem.* **1995**, *34*, 2265–2266.
 (29) Hikichi, S.; Ogihara, T.; Fujisawa, K.; Kitajima, N.; Akita, M.; Moro-oka, Y. *Inorg. Chem.* **1997**, *36*, 4539–4547.
 (30) Hegg, E. L.; Ho, R. Y. N.; Que, L., Jr. *J. Am. Chem. Soc.* **1999**, *121*, 1972–1973.
 (31) Chiou, Y.-M.; Que, L., Jr. *Angew. Chem., Int. Ed. Engl.* **1994**, *33*, 1886–1888.
 (32) Armarego, W. L. F.; Perrin, D. D. *Purification of Laboratory Chemicals*, 4th ed.; Butterworth-Heinemann: Oxford, 1997.
 (33) Kitajima, N.; Fujisawa, K.; Fujimoto, C.; Moro-oka, Y.; Hashimoto, S.; Kitagawa, T.; Toriumi, K.; Tatsumi, K.; Nakamura, A. *J. Am. Chem. Soc.* **1992**, *114*, 1277–1291.
 (34) Pavia, D. L.; Lampman, G. M.; Kriz, G. S., Jr. *Introduction to Organic Laboratory Techniques*, 2nd ed.; Saunders College Publishing: Philadelphia, 1982.
 (35) Nimitz, J. S.; Mosher, H. S. *J. Org. Chem.* **1981**, *46*, 211–213.

Scheme 2. Proposed Mechanism for α -Keto Acid-Dependent Enzymes

(0.086 g, 0.50 mmol), was added to a milky white slurry of $\text{Fe}(\text{ClO}_4)_2 \cdot 8\text{H}_2\text{O}$ (0.20 g, 0.50 mmol) and KTp^{Ph_2} (0.35 g, 0.50 mmol) in MeOH (5 mL). The reaction mixture was stirred for 30 min at room temperature, and a purple precipitate was isolated by filtration. Red-violet needles of $\mathbf{1} \cdot 2\text{CH}_3\text{C}(\text{O})\text{CH}_3$, suitable for X-ray diffraction, were grown by dissolving the crude solid in acetone (40 mL), quickly filtering the solution, and allowing the solution to sit undisturbed for 24 h at room temperature. This procedure led to the isolation of 0.25 g (50%) of diffraction quality crystals. Anal. Calcd. for $\mathbf{1} \cdot 2\text{CH}_3\text{C}(\text{O})\text{CH}_3$, $\text{C}_{53}\text{H}_{39}\text{BFeN}_6\text{O}_3 \cdot 2\text{C}_3\text{H}_6\text{O}$: C, 71.53; H, 5.19; N, 8.48. Found: C, 71.60; H, 5.18; N, 8.62. UV-vis [λ_{max} , nm (ϵ , $\text{M}^{-1} \text{cm}^{-1}$) in C_6H_6] 480 (sh, 390), 531 (540), 584 (sh, 500).

[Fe(Tp^{Ph2})(p-X-BF)], (1-X). The other substituted X-BF compounds were synthesized in an analogous manner but with substituted benzoylformic acids. The free acids were deprotonated with sodium hydride immediately before use and used without further purification.

[Fe(Tp^{Ph2})(p-MeO-BF)], (1-OMe). Redissolving the crude solid in acetone and allowing the solution to remain undisturbed overnight affords diffraction quality red-violet plates. Anal. Calcd. for $\text{C}_{54}\text{H}_{41}\text{BFeN}_6\text{O}_3 \cdot \text{H}_2\text{O}$: C, 70.30; H, 4.70; N, 9.11. Found: C, 70.30; H, 4.73; N, 9.08. UV-vis [λ_{max} , nm (ϵ , $\text{M}^{-1} \text{cm}^{-1}$) in C_6H_6] 479 (sh, 430), 522 (560), 574 (sh, 460).

[Fe(Tp^{Ph2})(p-Me-BF)], (1-Me). The crude solid was dissolved in CH_2Cl_2 and filtered, and diethyl ether diffused into the saturated solution yielded red-violet needles. Anal. Calcd. for $\text{C}_{54}\text{H}_{41}\text{BFeN}_6\text{O}_3 \cdot 1.5\text{H}_2\text{O}$: C, 70.83; H, 4.84; N, 9.18. Found: C, 70.93; H, 4.38; N, 9.25. UV-vis [λ_{max} , nm (ϵ , $\text{M}^{-1} \text{cm}^{-1}$) in C_6H_6] 492 (sh, 430), 530 (560), 578 (sh, 500).

[Fe(Tp^{Ph2})(p-F-BF)], (1-F). The crude solid was dissolved in CH_2Cl_2 and filtered, and diethyl ether diffused into the saturated solution yielded red-violet needles. Anal. Calcd. for $\text{C}_{53}\text{H}_{38}\text{BFFeN}_6\text{O}_3 \cdot 0.5\text{H}_2\text{O}$: C, 70.61; H, 4.36; N, 9.32; F, 2.11. Found: C, 70.81; H, 4.76; N, 9.14; F, 1.75. UV-vis [λ_{max} , nm (ϵ , $\text{M}^{-1} \text{cm}^{-1}$) in C_6H_6] 494 (sh, 400), 534 (530), 585 (sh, 560).

[Fe(Tp^{Ph2})(p-Cl-BF)], (1-Cl). The crude solid was dissolved in CH_2Cl_2 and filtered, and then diethyl ether was diffused into the saturated solution to obtain purple needles. Anal. Calcd. for $\text{C}_{53}\text{H}_{38}\text{BClFeN}_6\text{O}_3 \cdot \text{CH}_2\text{Cl}_2$: C, 65.25; H, 4.06; N, 8.46; Cl, 10.70. Found: C, 65.37; H, 4.15; N, 8.70; Cl, 10.80. UV-vis [λ_{max} , nm (ϵ , $\text{M}^{-1} \text{cm}^{-1}$) in C_6H_6] 500 (sh, 470), 542 (620), 608 (sh, 580).

[Fe(Tp^{Ph2})(m-NO₂-BF)], (1-NO₂). The crude dark blue solid obtained was dissolved in CH_2Cl_2 , filtered to remove insoluble inorganic

salts, and then layered with diethyl ether at room temperature to afford tiny dark blue needles unsuitable for crystallographic analysis. Anal. Calcd. for $\text{C}_{53}\text{H}_{38}\text{BFFeN}_7\text{O}_5 \cdot \text{H}_2\text{O} \cdot \text{CH}_2\text{Cl}_2$: C, 63.43; H, 4.14; N, 9.59. Found: C, 63.59; H, 3.90; N, 9.85. UV-vis [λ_{max} , nm (ϵ , $\text{M}^{-1} \text{cm}^{-1}$) in C_6H_6] 504 (330), 553 (500), 614 (520).

[Fe(Tp^{Ph2})(PRV)] (2) was prepared following a modification of the published procedure.³⁶ The sodium salt of pyruvic acid, NaPRV, (0.055 g, 0.50 mmol) was added to a milky white slurry of $\text{Fe}(\text{ClO}_4)_2 \cdot 8\text{H}_2\text{O}$ (0.20 g, 0.50 mmol) and KTp^{Ph_2} (0.35 g, 0.50 mmol) in MeOH (5 mL). The reaction mixture was stirred for 30 min at room temperature, and the red-orange precipitate that was formed was collected by filtration. This solid was dissolved in a minimal amount of CH_2Cl_2 (5 mL), and the insoluble impurities were removed by filtration. Vapor diffusion of Et_2O into the saturated CH_2Cl_2 solution after 2 days resulted in orange blocks of **2** suitable for X-ray diffraction analysis. Yield: 0.25 g (62%). Anal. Calcd. for **2**, $\text{C}_{48}\text{H}_{37}\text{BFFeN}_6\text{O}_3$: C, 70.95; H, 4.60; N, 10.34. Found: C, 71.06; H, 4.72; N, 10.41. UV-vis [λ_{max} , nm (ϵ , $\text{M}^{-1} \text{cm}^{-1}$) in C_6H_6]: 441 (210), 479 (210), 525 (sh, 120).

[Fe(Tp^{Ph2})(O₂CC(O)CH(CH₃)₂)] (3). Sodium 3-methyl-2-oxobutanoate (0.069 g, 0.50 mmol) was added to a milky white slurry of $\text{Fe}(\text{ClO}_4)_2 \cdot 8\text{H}_2\text{O}$ (0.20 g, 0.50 mmol) and KTp^{Ph_2} (0.35 g, 0.50 mmol) in MeOH (5 mL). The reaction mixture was stirred for 30 min at room temperature, and the crude orange solid that formed was collected by filtration. Dissolving the crude solid in a minimal amount of CH_2Cl_2 , filtering off insoluble impurities, and vapor diffusion of diethyl ether into this solution afforded orange needles of **3**. Yield: 0.22 g (52%). Anal. Calcd. for **3**· H_2O , $\text{C}_{50}\text{H}_{41}\text{BFFeN}_6\text{O}_3 \cdot \text{H}_2\text{O}$: C, 69.95; H, 5.05; N, 9.79. Found: C, 70.15; H, 4.89; N, 9.79. UV-vis [λ_{max} , nm (ϵ , $\text{M}^{-1} \text{cm}^{-1}$) in C_6H_6]: 441 (220), 475 (210), 513 (sh, 140).

[Fe(Tp^{Ph2})(OBz)] (4) was prepared following a modification of the published procedure.³⁰ Sodium benzoate (0.072 g, 0.50 mmol) was added to a milky white slurry of $\text{Fe}(\text{ClO}_4)_2 \cdot 8\text{H}_2\text{O}$ (0.20 g, 0.50 mmol) and KTp^{Ph_2} (0.35 g, 0.50 mmol) in MeOH (5 mL). The reaction mixture was stirred for 2 h at room temperature, and the crude off-white solid that was formed was collected by filtration. Dissolving the crude solid in a minimal amount of CH_2Cl_2 , filtering off insoluble impurities, and layering acetonitrile onto this yellow solution at -20°C afforded colorless blocks of **4** suitable for X-ray diffraction. Yield: 0.12 g (38%). Anal. Calcd. for **4**· $0.5 \text{H}_2\text{O}$, $\text{C}_{52}\text{H}_{39}\text{BFFeN}_6\text{O}_2 \cdot 0.5\text{H}_2\text{O}$: C, 73.00; H, 4.71; N, 9.82. Found: C, 73.21; H, 4.65; N, 9.96.

[Fe(Tp^{Ph2})(OAc)(3,5-Ph₂pzh)] (5). KTp^{Ph_2} (1.4 g, 2.0 mmol) was stirred with 1.5 equiv of anhydrous $\text{Fe}(\text{OAc})_2$ (0.52 g, 3.0 mmol) in 10 mL of CH_3CN and 15 mL of CH_2Cl_2 for 2 days. The reaction mixture was filtered through Celite, and the filtrate was dried under vacuum.

(36) Ho, R. Y. N.; Mehn, M. P.; Hegg, E. L.; Liu, A.; Ryle, M. J.; Hausinger, R. P.; Que, L., Jr. *J. Am. Chem. Soc.* **2001**, *123*, 5022–5029.

Table 1. Summary of Crystallographic Data [Fe(Tp^{Ph2})(PRV)] (**2**), [Fe(Tp^{Ph2})(OBz)] (**4**), [Fe(Tp^{Ph2})(OAc)(3,5-Ph₂pzH)] (**5**), and [Fe(Tp^{Ph2})(OAc)(3,5-Ph₂pzH)] (**6**)

	2	4	5	6
empirical formula	C ₉₆ H ₇₄ B ₂ Fe ₂ N ₁₂ O ₆	C ₅₃ H ₄₁ BCl ₂ FeN ₆ O ₂	C ₆₂ H ₄₉ BFeN ₈ O ₂	C ₆₂ H ₄₈ BFeN ₈ O ₃
formula weight g/mol	1624.99	931.48	1004.75	1019.74
crystal habit, color	block, orange	block, colorless	block, colorless	block, green
crystal system	orthorhombic	triclinic	triclinic	triclinic
space group	<i>Pca</i> 2(1)	<i>P</i> 1	<i>P</i> 1	<i>P</i> 1
<i>a</i> (Å)	18.125(1)	8.944(1)	13.633(3)	13.4709(8)
<i>b</i> (Å)	16.326(1)	16.053(2)	14.154(4)	14.1891(9)
<i>c</i> (Å)	27.145(2)	17.941(2)	15.481(4)	15.3253(9)
α (deg)	90	112.102(2)	84.339(4)	83.057(1)
β (deg)	90	101.903(2)	66.223(4)	66.655(1)
γ (deg)	90	100.557(2)	67.251(4)	67.175(1)
<i>V</i> (Å ³)	8032.3(9)	2236.7(4)	2515.2(11)	2477.0(3)
<i>Z</i>	4	2	2	2
<i>D</i> _{calc} (g/cm ³)	1.344	1.383	1.327	1.367
temperature (K)	173(2)	173(2)	173(2)	173(2)
absorption (cm ⁻¹)	4.27	5.07	3.55	3.63
θ range (deg)	1.25–25.03	1.29–27.53	1.44–25.12	1.45–25.04
<i>hkl</i> ranges	–19 to 21, –19 to 18, –32 to 32	–11 to 11, –20 to 20, –23 to 23	–16 to 16, –16 to 16, –18 to 18	–16 to 16, –16 to 16, –18 to 18
no. of reflections collected	45542	24366	25118	24935
no. of unique reflections	13993 (<i>R</i> _{int} = 0.1014)	10127 (<i>R</i> _{int} = 0.0241)	8913 (<i>R</i> _{int} = 0.0359)	8743 (<i>R</i> _{int} = 0.0217)
observed reflections (<i>I</i> > 2σ(<i>I</i>)) ^a	6300	8385	6832	7164
parameters	860	600	676	684
<i>R</i> 1/ <i>wR</i> 2 (<i>I</i> > 2σ(<i>I</i>)) ^a	0.0633/0.1402	0.0392/0.0994	0.0361/0.0881	0.0408/0.1169
<i>R</i> 1/ <i>wR</i> 2 (all data)	0.1515/0.1631	0.0500/0.1043	0.0507/0.0932	0.0518/0.1250
goodness-of-fit on <i>F</i> ²	1.006	1.024	0.983	1.013
max/min peak (e/Å ³)	0.718/–0.361	0.421/–0.577	0.331/–0.278	0.389/–0.404

$$^a R1 = \sum ||F_o| - |F_c|| / \sum |F_o|. \quad wR2 = [\sum [w(F_o^2 - F_c^2)^2] / \sum [w(F_o^2)^2]]^{1/2} \quad \text{where } w = 1/(\sigma^2(F_o^2) + (a \times P)^2 + b \times P).$$

The pale yellow powder was dissolved in CH₂Cl₂, and the resulting solution was filtered and evaporated to dryness. The resultant powder was extracted with CH₃CN to yield a white powder. The powder was recrystallized from CH₂Cl₂/CH₃CN at –20 °C to afford colorless blocks. Yield: 0.82 g (41%). Anal. Calcd. for **5**, C₆₂H₄₉BFeN₈O₂: C, 74.11; H, 4.92; N, 11.15. Found: C, 73.85; H, 4.79; N, 11.17.

[Fe(Tp^{Ph2})(OAc)(3,5-Ph₂pzH)] (**6**) was prepared by oxygenation of a dichloromethane solution of the acetate compound **5** followed by slow evaporation to obtain dark green X-ray quality crystals. Anal. Calcd. for **6**, C₆₂H₄₈BFeN₈O₃: C, 73.20; H, 4.74; N, 10.99. Found: C, 72.99; H, 4.84; N, 11.06. UV–vis [*λ*_{max}, nm (ε, M⁻¹ cm⁻¹) in C₆H₆]: 650 (1400).

Crystallographic Studies. [Fe(Tp^{Ph2})(PRV)] (**2**), [Fe(Tp^{Ph2})(OBz)] (**4**), [Fe(Tp^{Ph2})(OAc)(3,5-Ph₂pzH)] (**5**), and [Fe(Tp^{Ph2})(OAc)(3,5-Ph₂pzH)] (**6**) were characterized using X-ray diffraction. Each crystal was attached to the tip of a glass capillary and mounted on a Siemens SMART Platform CCD diffractometer for data collection at 173(2) K using graphite-monochromated MoKα (*λ* = 0.71073 Å) radiation. An initial set of cell constants was calculated from reflections harvested from three sets of 20 frames. These initial sets of frames were oriented such that orthogonal wedges of reciprocal space were surveyed. This produced initial orientation matrices determined from 98 reflections for **2**, 146 reflections for **4**, 101 reflections for **5**, and 57 reflections for **6**. Crystallographic data and experimental conditions are summarized in Table 1. All non-hydrogen atoms were refined anisotropically, and hydrogen atoms were placed in ideal positions and refined as riding atoms with relative isotropic displacement parameters. The only exceptions were the hydride bound to the boron atom (in **4–6**) and H42a (in **5** and **6**) that were found from the E-map and allowed independent isotropic refinement. In **2**, a pseudo-inversion center found at *x* = 1/8 and *y* = 1/4 caused difficulties in determining the space group and also caused distinct correlation problems between corresponding atoms in the two independent molecules of the asymmetric unit (i.e., it adversely affected bond distances and angles as well as anisotropic displacement factors). The presence of a local center is common in the space group *Pca*2(1) and can lead to problems with least squares refinement.³⁷ Therefore, to alleviate such problems

restraints were used to average the corresponding 1,2 and 1,3 bond distances and thermal displacement parameters between the two molecules of the asymmetric unit.³⁸ In addition, the data suggest a commensurate modulation that is not relieved at higher temperatures. A dichloromethane molecule was disordered over two positions in **4**. The final full matrix least squares refinement converged to *R*1 = 0.0633 and *wR*2 = 0.1631 for **2**, *R*1 = 0.0392 and *wR*2 = 0.1043 for **4**, *R*1 = 0.0361 and *wR*2 = 0.0932 for **5**, and *R*1 = 0.0408 and *wR*2 = 0.1250 for **6**.

Physical Methods. Elemental analyses were determined either by Atlantic Microlab, Inc. or at an analytical facility at the Research Laboratory of Resource Utilization, Tokyo Institute of Technology. UV/vis spectra were recorded either on a HP 8452A diode-array spectrometer with a temperature-controlled bath set to 30.0 °C or on a Hi-Tech Scientific SF-61DX2 stopped-flow spectrophotometer with a temperature-controlled bath. ¹H and ¹³C NMR spectra were collected on a Varian VI-500 spectrometer at room temperature. Special care was taken to ensure that the delay between pulses was greater than five times the longest proton longitudinal relaxation time (*T*₁) for proper integration of the peaks. Electrochemical measurements were carried out under nitrogen at ambient temperatures in solutions of CH₂Cl₂ with 0.1 M (Bu₄N)(ClO₄) as the supporting electrolyte using a model CS-1200 computer controlled potentiostat (Cypress Systems). Cyclic voltammograms (CV) were obtained using a three-component system consisting of a glassy carbon working electrode, a platinum wire auxiliary electrode, and a Ag/Ag⁺ reference electrode. The ferrocenium/ferrocene couple was measured under the same conditions to correct for junction potentials both as an internal reference and as a separate solution. The potential values were corrected by assigning the ferrocenium/ferrocene

(37) Marsh, R. E.; Schomaker, V.; Herstein, F. H. *Acta Crystallogr. B* **1998**, *54*, 921–924.

(38) The presence of a pseudo-inversion center at *x* = 1/8 and *y* = 1/4 forced the use of a restraint/constraint model that maintained similar 1,2 and 1,3 bond distances. Release of this restraint diminished the chemical reasonableness of the result, in particular, the bond lengths and angles. Therefore, an average of the bond lengths and angles for the two independent molecules is discussed whenever reference is made to this molecule. A table with distances for each independent molecule is available in the Supporting Information (Table S1).

couple the value of 0.480 V versus SCE.³⁹ X-band EPR spectra were recorded using a Bruker E-500 spectrometer with sample temperature maintained at 20 K with an Oxford Instruments ESR-10 liquid helium cryostat. Spectra were collected using a time constant of 82 ms, a sweep time of 82 ms, a modulation amplitude of 10 G, a modulation frequency of 100 kHz, and a power of 0.2 mW to avoid saturation. The electrospray ionization mass spectral data for the oxidized compounds were obtained using an LCQ mass spectrometer (ThermoFinnigan) on CH₂Cl₂ solutions that were directly infused into the spectrometer via a syringe pump.

Resonance Raman spectra were collected on an Acton AM-506 spectrometer (1200-groove grating) using a Kaiser Optical holographic super-notch filter with a Princeton Instruments liquid N₂-cooled (LN-1100PB) CCD detector with 4 cm⁻¹ spectral resolution. The laser excitation lines were obtained with a Spectra Physics 2030-15 argon ion laser and a 375B CW dye (Rhodamine 6G). The Raman frequencies were referenced to indene, and the entire spectral range of 400–1700 cm⁻¹ was obtained by collecting spectra at 2–3 different frequency windows and splicing the spectra together, making sure the solvent peaks were aligned before splicing. The spectra were obtained with a power of 200 mW at 77 K using a backscattering geometry on samples frozen on a gold-plated copper coldfinger in thermal contact with a Dewar containing liquid N₂. Typical accumulation times were 16–32 min per frequency window. Curve fits (Gaussian functions) and baseline corrections (polynomial fits) were carried out using Grams/32 Spectral Notebook Version 4.04 (Galactic).

Kinetics Measurements. Distilled thiophene-free benzene was stored over 3A molecular sieves under nitrogen and passed through a column of activated alumina prior to use. Crystalline materials were dissolved in benzene at room temperature. Temperature dependent changes in the density of benzene and the solubility of oxygen have been reported previously, and corrections were made for these phenomena.^{40,41} The solubility of O₂ in benzene is reported to be 9.15 mM at 30 °C, and oxygen saturation is assumed in these experiments.⁴¹ However, to determine the molecularity of the reaction with respect to oxygen, lower oxygen concentrations were required. Stopped-flow methods were utilized to minimize equilibration of oxygen into the headspace. Taking into account the temperature dependent changes in the density of benzene and the changes in oxygen solubility, as well as the 1:1 mixing ratio in the stopped-flow experiments, the maximum accessible concentration of O₂ at 50 °C was approximately 4.5 mM. Solutions with lower dioxygen concentrations were prepared using gastight syringes of O₂ and N₂ saturated solutions that were added in known proportion to a third syringe. Since the concentration of dioxygen greatly exceeded that of the iron(II) precursor, it was assumed to be constant throughout the reaction. The kinetic curves obtained under pseudo-first-order conditions over five to seven half-lives were fit to eq 1.

$$A_t = A_\infty - (A_\infty - A_0) \exp(-k_{\text{obs}} t) \quad (1)$$

Alternatively, for the oxygen dependence, kinetic data from 25% of the first half-life were fit to a linear function giving dA/dt as the initial rate of absorbance change. All rates reported are the average of at least three different trials.

Results and Discussion

The mononuclear iron(II) complexes **1–4** were synthesized by addition of 1 equiv of the sodium salt of the desired α -keto acid or sodium benzoate to equimolar portions of Fe^{II}-(ClO₄)₂•8H₂O and KTp^{Ph₂} in methanol. The acetate complex **5** was prepared directly from metathesis of KTp^{Ph₂} and iron(II)

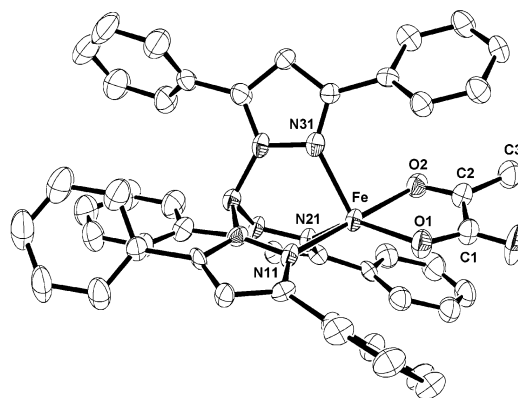


Figure 1. ORTEP plot of [Fe(Tp^{Ph₂})(PRV)] (**2**) showing 50% probability thermal ellipsoids and the labeling scheme for selected atoms. Hydrogen atoms are omitted for clarity.

acetate and was isolated as the pyrazole adduct. Although other workers have obtained related Fe^{II}(Tp^{R₁R₂}) complexes of carboxylates without an additional pyrazole ligand,^{29,42,43} the acetate complex could only be isolated as the pyrazole adduct. Addition of excess 3,5-diphenylpyrazole to the reaction mixture increased the yield of **5**.

Structures of Iron(II) Precursors. There are several previously reported examples of benzoylformate complexes,^{27,29,30} but the pyruvate compound **2** is the first fully characterized model compound to have an aliphatic α -keto carboxylate ligand, similar to the cofactors in the enzymatic systems. The crystal structure of **2** reveals a five-coordinate iron(II) center with a monoanionic face-capping Tp^{Ph₂} and a chelated pyruvate (Figure 1 and Table 2), comparable to those observed for five-coordinate chelated benzoylformate complexes. The iron centers of both [Fe(Tp^{Ph₂})(BF)] (**1**) and [Fe(Tp^{Ph₂})(PRV)] (**2**) are best described as distorted trigonal bipyramids ($\tau = 0.65$ and 0.67 , respectively).^{44,45} In both cases, the principal axis through the iron(II) center is defined by the α -keto carbonyl oxygen and the nitrogen of the most weakly bound pyrazole (N2–Fe–O2 = 171.7(2) for **1** and N11–Fe–O2 179.2(3) for **2**), while the more strongly bound carboxylate oxygen and the remaining pyrazole nitrogens define the trigonal plane. The pyrazole bond lengths are typical of Tp^{R₁R₂} complexes of high-spin iron(II),^{29,30,42} and the absence of a counterion confirms that the α -keto acid binds as the conjugate base. The C2–C3 bond length (1.498(9) Å) of the pyruvate complex **2** is typical for a C–C single bond and inconsistent with binding of the enolate tautomer.²⁷ Furthermore, the two distinct Fe–O bond lengths of 1.967(5) and 2.242(6) Å associated with Fe–O_{carboxylate} and Fe–O_{keto} bonds, respectively, are comparable to the distances observed in the benzoylformate compounds (**1**, 1.968(4) and 2.206(5) Å; [Fe(Tp^{tBu,iPr})(BF)], 1.975(7) and 2.261(7); and [Fe(6-Me₃-TPA)-(BF)]⁺, 2.001(4) and 2.212(4) Å, respectively).^{27,29,30} As with the other complexes, the five-membered chelate ring of the pyruvate complex is nearly planar with no torsion angle over two degrees. These structures can be compared with those

(42) Kitajima, N.; Tamura, N.; Amagai, H.; Fukui, H.; Moro-oka, Y.; Mizutani, Y.; Kitagawa, T.; Mathur, R.; Heerwegh, K.; Reed, C. A.; Randall, C. R.; Que, L., Jr.; Tatsumi, K. *J. Am. Chem. Soc.* **1994**, *116*, 9071–9085.

(43) Ogihara, T.; Hikichi, S.; Akita, M.; Uchida, T.; Kitagawa, T.; Moro-oka, Y. *Inorg. Chim. Acta* **2000**, *297*, 162–170.

(44) Addison, A. W.; Rao, T. N.; Reedijk, J.; van Rijn, J.; Verschoor, G. C. *J. Chem. Soc., Dalton Trans.* **1984**, 1349–1356.

(45) In this convention, a perfect square pyramid would have a τ value of 0.00, and a trigonal bipyramid would have a τ value of 1.00.

(39) Connelly, N. G.; Geiger, W. E. *Chem. Rev.* **1996**, *96*, 877–910.

(40) Lide, D. R.; Kehiaian, H. V. *CRC Handbook of Thermophysical and Thermochemical Data*; CRC Press: Boca Raton, 1994.

(41) Battino, R. *Solubility Data Series*; Pergamon Press: Oxford, 1981; Vol. 7, pp 250–255.

Table 2. Selected Bond Lengths (Å) for **1**, **2**, **4**, **5**, Comparisons with Reported Compounds, and **6**

	1 ^a	2	[Fe(Tp ^{Bu,Pr})(BF)] ^b	[Fe(Tp ^{Bu,Pr})(η ¹ -BF)(3-Pr-5-fBupzH)] ^b	4	5	[Fe(Tp ^{Pr2})(OAc)] ^c	6
Fe–O1	1.968(4)	1.967(5)	1.975(7)	2.003(8)	2.0028(12)	1.9634(14)	2.234(3)	1.9740(16)
Fe–O2	2.206(5)	2.242(6)	2.261(7)		2.3449(12)		2.060(3)	
Fe–O3								1.8877(14)
Fe–N11 [N2] [#]	2.188(5) [#]	2.163(6)	2.116(9)	2.271(9)	2.1762(13)	2.2626(15)	2.073(3)	2.2022(17)
Fe–N21 [N4] [#]	2.068(5) [#]	2.088(8)	2.173(9)	2.117(9)	2.0916(14)	2.0745(15)	2.093(2)	2.1652(17)
Fe–N31 [N6] [#]	2.086(5) [#]	2.106(8)	2.112(9)	2.102(8)	2.0653(13)	2.0855(16)	2.092(3)	2.0654(17)
Fe–N41				2.22(1)	2.2347(17)		2.2344(17)	
C1–O1	1.286(7)	1.279(8)	1.27(1)	1.26(1)	1.285(2)	1.263(2)	1.230(5)	1.201(3)
C1–O2					1.240(2)	1.237(3)	1.268(5)	1.251(3)
C2–O2	1.237(8)	1.233(7)	1.24(1)	1.20(1)				
C1–C2 [C46–C47] [#]	1.532(9) [#]	1.557(9)	1.59(1)	1.53(2)	1.493(2)	1.505(3)	1.506(5)	1.528(3)
C2–C3		1.498(9)						
O3–C136								1.339(3)
τ ^d	0.65	0.67	0.78	0.33	0.65	0.32	0.17	
BVS ^e	1.93	1.89	1.81	2.34	1.82	1.90	1.89	2.86

^a Reference 30. ^b Reference 29. ^c Reference 42. ^d Reference 44. ^e Reference 46.

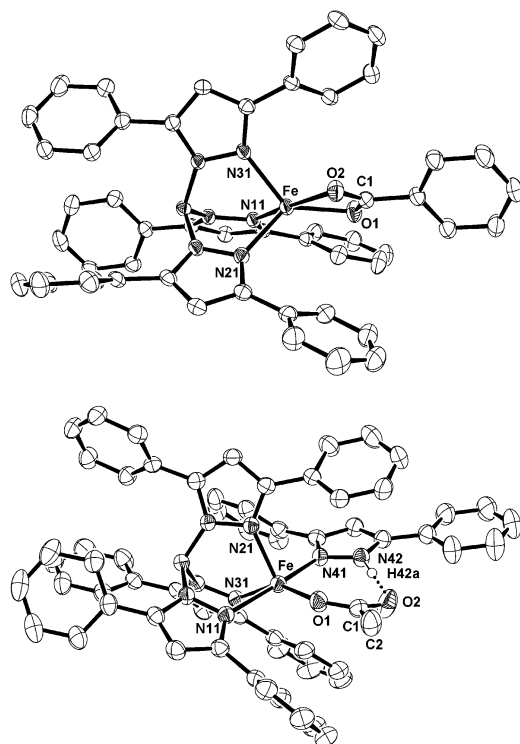


Figure 2. ORTEP plots of [Fe(Tp^{Ph2})(OBz)] (**4**) and [Fe(Tp^{Ph2})(OAc)(3,5-Ph₂pzh)] (**5**) showing 50% probability thermal ellipsoids and the labeling scheme for selected atoms. The dashed line shows the hydrogen-bonding interaction between H42a on the free pyrazole and O2 of the acetate anion. The dichloromethane (in **4**) and all other hydrogen atoms are omitted for clarity.

recently reported for α -KG-dependent iron(II) enzymes with bound cofactor and substrate.^{17,19,20} While all three show a chelated α -ketoglutarate, the iron center of anthocyanidin synthase has a water molecule occupying the sixth site to give a distorted octahedral geometry,¹⁹ and the other two (DAOCS and TauD) have a distorted square pyramidal geometry ($\tau = 0.26$ ¹⁷ and 0.12²⁰) about the iron(II) center.

To examine the importance of the α -keto carboxylate, two corresponding carboxylate compounds have also been synthesized (Figure 2 and Table 2). The iron center of the benzoate complex **4** has a distorted trigonal bipyramidal coordination geometry ($\tau = 0.65$) in which the axial ligands are the most weakly bound pyrazole N11 and benzoate oxygen O2 (N11–

Fe–O2 = 171.33(4)^o). The remaining ligands define the equatorial plane. The pyrazole bond lengths are typical for a high-spin iron(II) center. The carboxylate is chelated asymmetrically to the iron center (Fe–O1 = 2.0028(12) and Fe–O2 = 2.3449(12)), as observed in related bidentate carboxylate complexes. For example, the five-coordinate iron(II) compounds [Fe(Tp^{iPr2})(OAc)] and [Fe(Tp^{Bu,iPr})(OAc)] have iron–oxygen bond lengths of 2.060(3) and 2.234(3) Å, and 2.080(3) and 2.233(3) Å, respectively.^{42,43} In fact, the benzoate ligand in **4** exhibits the largest asymmetry, $\Delta r_{\text{Fe–O}} = 0.34$ Å. Furthermore, the iron–oxygen bond lengths in the benzoate complex **4** are significantly longer than the 1.889(6) Å distance reported for [Fe(Tp^{Bu,iPr})(η¹-BF)(CH₃CN)], a five-coordinate iron(II) complex with a monodentate benzoate.²⁹

In contrast, complex **5** has a monodentate acetate ligand and is crystallized as the 3,5-diphenylpyrazole adduct. The coordination geometry for the iron(II) acetate complex **5** is best described as a distorted square pyramid ($\tau = 0.32$) with one nitrogen from the Tp^{Ph2} ligand in the apical position (N21). The pseudo-basal plane is composed of the two remaining pyrazoles from the face-capping ligand, the neutral pyrazole, and the monodentate acetate. The most weakly bound pyrazole of the Tp^{Ph2} ligand is trans to the neutral 3,5-diphenylpyrazole (N11–Fe–N41 = 170.20(5)^o). The shortest bond is the Fe–O1 bond (1.963(1) Å). The carbonyl oxygen O2 of the acetate anion is 2.682(3) Å from the nitrogen of the neutral pyrazole N42, suggesting a hydrogen-bonding interaction. The interaction also brings the acetate and the neutral pyrazole nearly coplanar (torsional angle N41–N42–O2–O1 = 16.4(1)^o).

The structures of **2**, **4**, and **5** consist of an [Fe(Tp^{Ph2})]⁺ unit coordinated by a monoanionic ligand that gives rise to a five-, four-, or seven-membered chelate ring, respectively. Despite the differences in bite angle (O1–Fe–O2 = 77.0(3)^o for **2** and 59.96(4)^o for **4**), the iron(II) centers of **2** and **4** are both distorted trigonal bipyramids with similar degrees of trigonality ($\tau = 0.67$ for **2** and 0.65 for **4**). In contrast, **5** has a square pyramidal metal center ($\tau = 0.32$). If the hydrogen-bonding interaction between the acetate and the pyrazole is considered to give rise to a seven-membered chelate ring, then the acetate-pyrazole unit has a much larger bite angle (O1–Fe–N41 = 102.08(6)^o) affording a metal center with a lower τ value. The steric bulk of 3,5-diphenylpyrazole may also contribute to the preference for a square pyramidal geometry. Thus, there appears to be a

Table 3. Properties of Iron(II) Precursors^a

cpd	UV/vis ^b			¹ H NMR parameters ^c					Electrochemistry ^d	
	λ_{\max} , nm (ϵ , M ⁻¹ cm ⁻¹)			4-pz δ (ppm)	<i>o</i> -3-Ph δ (ppm)	<i>m</i> -3-Ph δ (ppm)	<i>p</i> -3-Ph δ (ppm)	-R δ (ppm)	E_{pa} (mV)	$E_{1/2}$ (mV)
1-OMe	479 (430)	522 (560)	574 (460)	60 (5.2)	-21 (0.4)	7.9 (4.9)	7.0 ^e	19 (<i>o</i> , 4.1) 7.8 (<i>m</i> , 15) 2.9 (<i>p</i> -OCH ₃ , 130)	890	-1330
1-Me	492 (430)	530 (560)	578 (500)	60 (5.9)	-20 (0.4)	7.8 (7.5)	7.0 ^e	19 (<i>o</i> , 3.7) 7.9 (<i>m</i> , 19) -4.1 (<i>p</i> -CH ₃ , 111)	920	-1270
1	480 (390)	531 (540)	584 (500)	60 (5.6)	-20 (0.4)	8.0 (7.8)	7.0 (7.1)	19 (<i>o</i> , 3.4) 7.9 (<i>m</i> , 25) 13.6 (<i>p</i> , 71)	930	-1220
1-F	494 (400)	534 (530)	585 (460)	59 (6.0)	-19 (0.4)	8.0 (7.6)	7.0 ^e	19 (<i>o</i> , 3.4) 7.5 (<i>m</i> , 55)	960	-1230
1-Cl	500 (470)	542 (620)	596 (580)	59 (6.1)	-19 (0.5)	8.0 (6.6)	7.0 ^e	19 (<i>o</i> , 3.7) 7.6 (<i>m</i> , 37)	970	-1150
1-NO ₂	504 (330)	553 (500)	614 (522)	61 (5.6)	-17 (0.4)	8.1 (5.3)	6.9 ^e	25 (<i>o'</i> , 4.0) 14.4 (<i>o</i> , 5.4) 9.1 (<i>m</i> , 31) 14.2 (<i>p</i> , 77)	1010	
2	441 (210)	479 (210)	525 (120)	60 (6.1)	-20 (0.5)	8.0 (6.6)	7.8 (4.8)	7.3 (4.8)	980	-1630
3	441 (220)	475 (210)	513 (140)	60 (5.7)	-21 (0.5)	7.8 (6.1)	7.1 ^e	30 (C-H, 2.8) 3.0 (CH ₃ , 5.9)	1000	-1670
4				60 (15)	-16 (1.4)	7.2 (24)	6.8 (55)	29 (<i>o</i> , 6.3) 16 (<i>m</i> , 65) 7.1 (<i>p</i> , 108)	870, 1320	
5				57 (5.3)	-6.5 (2.7)	7.6 (8.5)	6.7 (7.0)	77 (1.7)	830, 1070	

^a **1** = [Fe(Tp^{Ph2})(BF)]; **2** = [Fe(Tp^{Ph2})(PRV)]; **3** = [Fe(Tp^{Ph2})(O₂CC(O)CH(CH₃)₂)]; **4** = [Fe(Tp^{Ph2})(OBz)]; and **5** = [Fe(Tp^{Ph2})(OAc)(3,5-Ph₂pzh)]. Numbers in parentheses are relaxation times (T_1) in milliseconds. ^b In C₆H₆. ^c In C₆D₆. ^d Cyclic voltammograms in CH₂Cl₂ with 0.1 M Bu₄N(ClO₄) at 100 mV/s. ^e Too close to solvent to be determined.

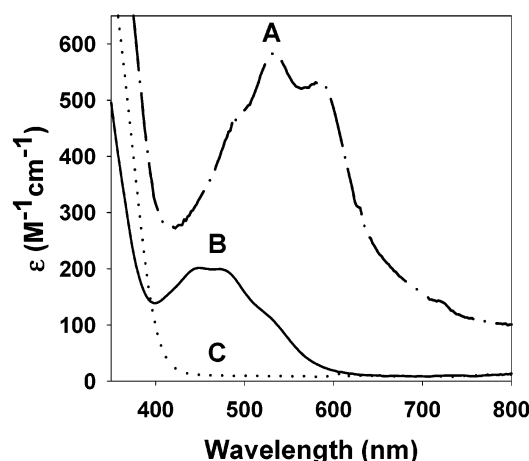


Figure 3. Electronic spectra of α -keto carboxylate and carboxylate complexes recorded at 30.0 °C in benzene. (A) [Fe(Tp^{Ph2})(BF)] (**1**) (---); (B) [Fe(Tp^{Ph2})(PRV)] (**2**) (—); and (C) [Fe(Tp^{Ph2})(OBz)] (**4**) (···).

very sensitive interplay between the steric bulk of the mono-anionic ligands and alkyl substitution of the tris(pyrazolyl)borate ligand. For example, with the [Fe(Tp^{iBu,iPr})]⁺ fragment, the acetate complex is square pyramidal while the larger benzoylformate anion results in a trigonal bipyramidal geometry about the iron center; in fact, the latter converts to a tetrahedral complex with a monodentate benzoylformate ligand at high temperature.^{29,43} This suggests that the steric bulk of the [Fe(Tp^{Ph2})]⁺ framework is reduced as compared to [Fe(Tp^{iBu,iPr})]⁺ or [Fe(Tp^{iPr2})]⁺, consistent with the series for effective steric bulk of substituted tris(pyrazolyl)borate ligands proposed by Kitajima and Tolman.⁴⁷

Properties of Iron(II) Precursors. Complexes **1–X** exhibit a visible chromophore characteristic of an iron(II)-bidentate α -keto acid unit (Figure 3, Table 3).^{27,36,48} These blue-purple complexes show three absorption features (Figure 3A) assigned to metal-to-ligand charge transfer transitions based on similarity to the previously reported compounds [Fe(6-Me₃-TPA)(BF)]⁺,

[Fe(Tp^{Me2})(BF)], and [Fe(Tp^{iBu,iPr})(BF)].^{27–29} Support for this assignment comes from the substituted benzoylformate complexes (**1–X**), in which electron-releasing groups lead to higher energy charge-transfer bands while electron-withdrawing substituents lead to lower energy bands. The shift in energy of the most intense charge-transfer transition correlates well with the Hammett parameter σ ($R^2 = 0.96$, Figure S1, Supporting Information). This assignment is supported by density functional calculations on an iron(II)-pyruvate fragment.⁴⁸

On the other hand, the aliphatic α -keto carboxylate complexes **2** and **3** are red-orange and exhibit three transitions centered near 470 nm (Figure 3B). The observed blue shift is consistent with their assignment as metal-to-ligand charge-transfer bands, as replacement of the phenyl group with the more electron-donating methyl group would lead to higher energy π^* orbitals on the α -keto acid ligand. Furthermore, they also differ from **1** in absorption intensity, their extinction coefficients (220 M⁻¹ cm⁻¹) being less than half those reported for the benzoylformate compounds (~ 540 M⁻¹ cm⁻¹). We attribute this difference to conjugation of the α -keto acid chromophore with the aromatic ring, which is nearly coplanar with the chelated α -keto carboxylate in **1**. The lower absorptivities of **2** and **3** are comparable to those observed for the α -KG complexes of CAS and TauD.^{48,49} In contrast, the benzoate and acetate complexes **4** and **5** exhibit no transitions in the visible region (Figure 3C). Therefore, the α -keto group is necessary to elicit a charge-transfer band in the visible region.

The ¹H NMR spectra of these paramagnetic high-spin iron(II) complexes are useful for assessing the extent to which the solid-state structures are maintained in solution (Figure 4). In noncoordinating solvents such as benzene or dichloromethane, the α -keto carboxylate compounds undergo no noticeable change in color from the solid state to solution, suggesting that they remain five-coordinate. The NMR peaks for the iron(II) compounds have been assigned based on chemical shift, relative integration, longitudinal relaxation times (T_1), ¹H,¹H COSY cross-peaks observed, and comparisons with previously reported tris(pyrazolyl)borate compounds (Table 3, Figures S2 and S3;

(46) Liu, W.; Thorp, H. H. *Inorg. Chem.* **1993**, *32*, 4102–4105.

(47) Kitajima, N.; Tolman, W. B. *Prog. Inorg. Chem.* **1995**, *43*, 419–531.

(48) Pavel, E. G.; Zhou, J.; Busby, R. W.; Gunsior, M.; Townsend, C. A.; Solomon, E. I. *J. Am. Chem. Soc.* **1998**, *120*, 743–753.

(49) Ryle, M. J.; Padmakumar, R.; Hausinger, R. P. *Biochemistry* **1999**, *38*, 8, 15278–15286.

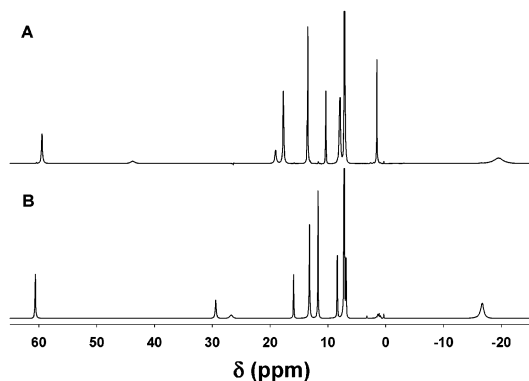


Figure 4. ¹H NMR spectrum of (A) [Fe(Tp^{Ph2})(BF)] (**1**) and (B) [Fe(Tp^{Ph2})(OBz)] (**4**) in benzene-*d*₆ at room temperature. Spectra are referenced to the residual protic solvent peak at 7.16 ppm. Despite prolonged exposure of the solid to vacuum, a resonance from acetone at 1.9 ppm is also visible in panel A.

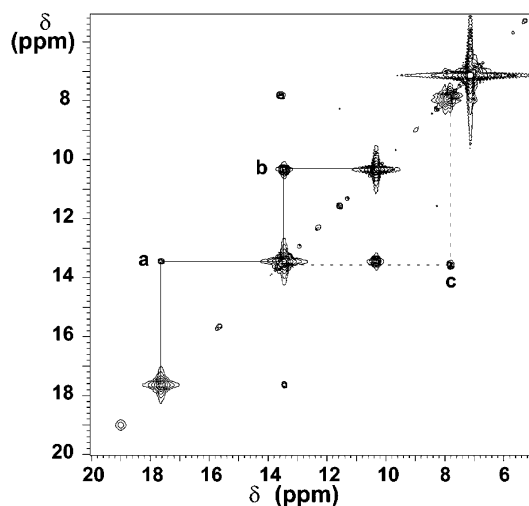


Figure 5. ¹H, ¹H COSY spectrum of **1** in benzene-*d*₆ at room temperature. Solid lines indicate the cross couplings in the 5-phenyl protons, and a dashed line indicates the cross-peak for the benzoylformate protons.

see Table S2 for full table). In all cases, the tris(pyrazolyl)-borate arms are magnetically equivalent in solution.

The assignments for [Fe(Tp^{Ph2})(BF)] in C₆D₆ will be discussed as a representative example of the assignment process (Figure 4A), beginning with the resonances of the Tp^{Ph2} protons. In the spectrum of **1**, the peak with the largest downfield shift (60 ppm) has an integration of 3 protons and a short *T*₁ of 5.6 ms; it is assigned to the 4-hydrogen of the pyrazole ring, in accordance with the observed properties of 4-pyrazole protons in other Fe(Tp^{R1,R2}) complexes ($\delta \sim 60\text{--}65$ ppm, 3H).^{29,42} The very broad peak (*T*₁ = 1.1 ms) at 44 ppm is assigned to the B–H proton, as compared to 28 ppm for the B–H proton observed for [Fe(Tp^{iBu,iPr})(OAc)] in C₆D₆.²⁹ The furthest upfield peak ($\delta = -20$ ppm) has a very short *T*₁ of 0.4 ms and is assigned to the ortho protons of the 3-phenyl group because of their proximity to the metal center. On the basis of its integration and *T*₁, the peak at 7.0 ppm (*T*₁ = 7.1 ms) is the only candidate for the para proton of the 3-phenyl, while the resonance at 8.0 ppm (*T*₁ = 7.8 ms) is assigned to the meta protons of the 3-phenyl ring. The protons of the 5-phenyl group are interrelated by cross-peaks *a* and *b*, which connect resonances at 18, 13.5, and 10.4 ppm into one spin system (Figure 5, solid lines) and identify them as the ortho, meta, and para protons of the

5-phenyl group, respectively. A similar shift pattern is observed for the Tp^{Ph2} protons of **1-X** and **2-5** (Tables 3 and S2).

The resonances of the benzoylformate protons of **1** are assigned to the remaining unassigned peaks at 19, 13.6, and 7.9 ppm. Cross-peak *c* in Figure 5 connects the resonances at 13.6 and 7.9 ppm. Relative integrations require the peak at 13.6 ppm to be the para proton coupled to the meta proton at 7.9 ppm, so the remaining two-proton resonance at 19 ppm must be assigned to the ortho protons. A cross-peak is not observed between the meta and ortho protons because of the short relaxation time for the ortho protons (*T*₁ = 3.4 ms). It is noteworthy that the benzoylformate phenyl ring protons exhibit an alternating shift pattern indicative of a dominant π -spin delocalization pathway, while the 5-phenyl protons exhibit a pattern of decreasing downfield shifts consistent with a dominant σ -delocalization pathway.^{50,51} A similar pattern of shifts is observed for the protons of other bidentate benzoylformate complexes (**1-X**) exhibit chemical shifts for the phenyl ring that are consistent with these assignments (Tables 3 and S2).

As expected, the signals associated with the benzoylformate protons in **1** are absent in the spectra of **2** and **3** (Table 3, Figure S2). Instead in **2** there is a peak at 7.3 ppm with a short relaxation time (*T*₁ = 4.8 ms) that can be assigned to the pyruvate methyl group. Curiously, the isopropyl methine proton in **3** appears at 30 ppm. In both molecules, this position is four bonds removed from the iron(II) center and should be affected similarly by spin polarization and spin delocalization mechanisms. The larger shift of the methine proton may be attributed to preferred conformations or restricted rotation of the isopropyl in which the unpaired spin density on the p_{π} orbital of the α -keto carbon is more effectively transmitted to the isopropyl methine proton via hyperconjugation. Similar effects have been observed in a number of systems with restricted rotation.^{52–54} This observation suggests the bulk of the Tp^{Ph2} ligand may have some influence on the preferred orientation of the isopropyl group.

The carboxylate complexes **4** and **5** exhibit similar ¹H NMR shift patterns and relaxation parameters (Table 3, Figure 4B). Complex **4** exhibits new resonances at 29, 16, and 7.1 ppm that can be assigned to the benzoate ortho, meta, and para protons, respectively. The connectivity between the latter two is established by the observation of a COSY peak (*c* in Figure S3). The paramagnetic shift falls off and the relaxation time increases with the distance from the iron(II) center for the benzoate protons, indicative of a dominant σ -bond spin delocalization pathway.^{50,51} These resonances are replaced by a broad peak at 77 ppm in **5**, assigned to the acetate methyl group. This value is comparable to that observed for [Fe(Tp^{iBu,iPr})(OAc)], which has been isolated with and without an additional pyrazole ligand; the acetate protons shift from 119 to 95 ppm upon introduction of the neutral pyrazole.²⁹ In the case of [Fe(Tp^{iBu,iPr})(OAc)], the added pyrazole also appears in the diamagnetic region of

(50) Bertini, I.; Luchinat, C. *NMR of Paramagnetic Molecules in Biological Systems*; Benjamin/Cummings Publishing Co., Inc.: Menlo Park, CA, 1986.

(51) Ming, L.-J. in *Physical Methods in Bioinorganic Chemistry: Spectroscopy and Magnetism*; Que, L., Jr., Ed.; University Science Books: Sausalito, CA, 2000.

(52) Ming, L.-J.; Lauffer, R. B.; Que, L., Jr. *Inorg. Chem.* **1990**, *29*, 3060–3064.

(53) Scarow, R. C.; Pyrz, J. W.; Que, L., Jr. *J. Am. Chem. Soc.* **1990**, *112*, 657–665.

(54) La Mar, G. N.; Horrocks, W. D., Jr.; Holm, R. H. *NMR of Paramagnetic Molecules; Principles and Applications*; Academic Press: New York, 1973; p 678.

the spectrum; however, similar peaks have not been observed for the neutral pyrazole in $[\text{Fe}(\text{Tp}^{\text{Ph}_2})(\text{OAc})(3,5\text{-Ph}_2\text{pzH})]$, suggesting that it may be in an intermediate exchange regime.

The electrochemical properties of the iron(II) precursors have been examined by cyclic voltammetry of anaerobic dichloromethane solutions with tetrabutylammonium perchlorate as the supporting electrolyte (Table 3). Complex **1** shows an anodic one-electron wave at 930 mV versus SCE, corresponding to the oxidation of iron(II). There is a cathodic wave at 770 mV versus SCE but with a smaller current, suggesting an irreversible change after oxidation to iron(III). Substitution of the benzoylformate group results in the modulation of this potential from 890 to 1010 mV versus SCE. The other α -keto carboxylate compounds show similar anodic peaks at 980 mV for **2** and 1000 mV for **3**, while the carboxylate compounds exhibit multiple irreversible waves (**4**, $E_{\text{pa}} = 870$ and 1320 mV, **5** 830 and 1070 mV versus SCE). It is interesting to note that all five complexes have $\text{Fe}^{\text{III}}/\text{Fe}^{\text{II}}$ potentials near 1 V despite the fact that carboxylates are much stronger bases than α -keto carboxylates ($\text{p}K_{\text{a}} = 4.19$ and 4.75^{55} for benzoic acid and acetic acid, respectively, vs 1.39^{56} (or 1.1^{57}) and 1.94^{58} for benzoylformic and pyruvic acid, respectively).

For **1–3**, there is an additional quasi-reversible wave that can be assigned to the formation of a ketyl anion radical. The ketone/ketyl couple is observed at -1220 mV versus SCE ($\Delta E = 160$ mV) for **1** and is shifted to -1630 mV versus SCE ($\Delta E = 210$ mV) for **2**, and -1670 mV versus SCE ($\Delta E = 210$ mV) for **3**. Substitution of the benzoylformate ring also affects this couple, and while **1-NO₂** exhibits irreversible waves, more electron-releasing groups result in cathodic shifts of the ketone/ketyl couple (Figure S4). The cathodic shift of the ketyl couple suggests the π^* -acceptor orbital of the BF ligand in **1** is stabilized relative to those of the α -keto acid ligands in **2** and **3**, probably because of conjugation with the phenyl ring. This trend is consistent with the blue shifts in the MLCT transitions observed for **2** and **3**. The conjugation may also stabilize the dianionic enolate form of BF and rationalize the lower $\text{Fe}^{\text{III}}/\text{Fe}^{\text{II}}$ potential of **1** relative to **2** and **3**.

Oxygenation of Iron(II) Precursors. Despite the very positive $\text{Fe}^{\text{III}}/\text{Fe}^{\text{II}}$ potentials, **1–5** all react with dioxygen to generate a green species (Figure 6), in which the ortho carbon of one 3-phenyl group has been hydroxylated. This iron(III) phenolate product is formulated as $[\text{Fe}(\text{Tp}^{\text{Ph}_2})(\text{O}_2\text{CR})]$ ($\text{R} = \text{Ph}, \text{Me}, \text{Pr}$) and has been crystallized from the reaction of the acetate complex **5**, as the 3,5-diphenylpyrazole adduct (**6**) (Figure 7, Table 2). The geometry about the iron center is a distorted octahedron with one face capped by the tris(pyrazolyl)borate ligand. The ortho carbon of one 3-phenyl group has been hydroxylated, and the phenolate oxygen is bound to the metal center. A monodentate acetate and a 3,5-diphenylpyrazole complete the metal coordination sphere. As in the structure of **5**, a rather short N42–O2 distance of $2.684(3)$ Å indicates hydrogen bonding between the pyrazole and the acetate. This interaction makes the two components nearly coplanar with a N41–N42–O2–O1 torsion angle of $16.0(0.2)^\circ$. The hydroxy-

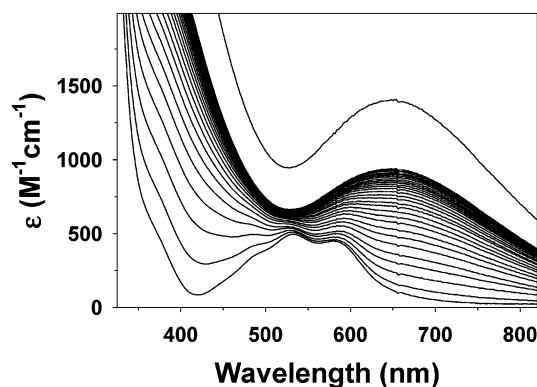


Figure 6. Electronic spectra of $[\text{Fe}(\text{Tp}^{\text{Ph}_2})(\text{BF})]$ (**1**) in benzene upon exposure to O_2 (cycle time 2 min) for 1 h at 30.0 °C as compared with the electronic spectrum of crystalline $[\text{Fe}(\text{Tp}^{\text{Ph}_2})(\text{OAc})(3,5\text{-Ph}_2\text{pzH})]$ (**6**) in CH_2Cl_2 .

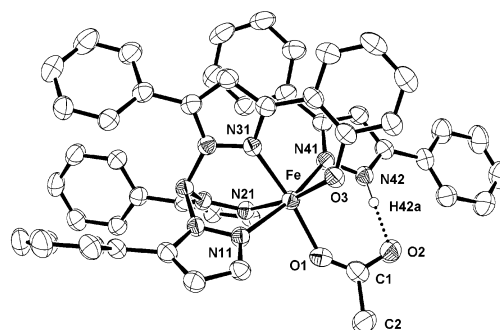


Figure 7. ORTEP plot of $[\text{Fe}(\text{Tp}^{\text{Ph}_2})(\text{OAc})(3,5\text{-Ph}_2\text{pzH})]$ (**6**) showing 50% probability thermal ellipsoids and the labeling scheme for selected atoms. The dashed line shows the hydrogen-bonding interaction between H42a on the free pyrazole and O2 of the acetate anion. All other hydrogen atoms as well as the two unmodified phenyl rings at the 3-position of the pyrazolyl borate ligand are omitted for clarity.

lated arene, constrained by binding to the iron center, is also nearly coplanar with the pyrazole ring to which it is attached. The two aromatic rings show a torsional angle of less than 10° . The phenolate oxygen has the strongest bond to the iron(III) center ($\text{Fe}-\text{O}_3 = 1.888(1)$ Å), a value comparable to those of other iron(III) phenolate complexes.^{59–62} The $\text{Fe}-\text{N}31$ bond length of $2.0654(17)$ Å is also much shorter than those of the other pyrazole ligands (av 2.20 Å), reflecting the constraints imposed by this six-membered chelate ring.

The $[\text{Fe}(\text{Tp}^{\text{Ph}_2})(\text{O}_2\text{CR})]$ moiety has also been characterized by a number of spectroscopic techniques. It exhibits an intense signal at $g = 4.3$ typical of an iron(III) center in a rhombic environment (Figure S5). Electrospray mass spectra show a major ion at $m/z = 740$ (Figure 8A), corresponding to $[\text{Fe}^{\text{III}}(\text{Tp}^{\text{Ph}_2})]^+$, with an isotope distribution pattern that closely mirrors that calculated for this fragment. The characteristic dark green color of $[\text{Fe}(\text{Tp}^{\text{Ph}_2})(\text{O}_2\text{CR})]$ corresponds to a visible band at 650 nm ($\epsilon = 1400$ $\text{M}^{-1} \text{cm}^{-1}$) assigned as a phenolate-to-iron(III) charge-transfer transition.^{60,62,63} This band is unaffected by the nature of the carboxylate ($-\text{Me}$, $-\text{Ph}$, $-\text{Pr}$). Excitation into the phenolate-to-iron(III) charge-transfer band of $[\text{Fe}(\text{Tp}^{\text{Ph}_2})(\text{O}_2-$

(55) Lide, D. R. *CRC Handbook of Chemistry and Physics*; 73rd ed.; CRC Press: Boca Raton, FL, 1992; pp 8–39.
 (56) Wheatley, M. S. *Experientia* **1956**, *12*, 339–340.
 (57) Kuhn, H. J.; Görner, H. *J. Phys. Chem.* **1988**, *92*, 6208–6219.
 (58) Chiang, Y.; Kresge, A. J.; Pruszyński, P. *J. Am. Chem. Soc.* **1992**, *114*, 3103–3107.

(59) Heistand, R. H., II; Roe, L.; Que, L., Jr. *Inorg. Chem.* **1982**, *21*, 676–681.
 (60) Yan, S.; Pan, X.; Taylor, L. F.; Zhang, J. H.; O'Connor, C. J.; Britton, D.; Anderson, O. P.; Que, L., Jr. *Inorg. Chim. Acta* **1996**, *243*, 1–8.
 (61) Ainscough, E. W.; Brodie, A. M.; Plowman, J. E.; Brown, K. L.; Addison, A. W.; Gainsford, A. R. *Inorg. Chem.* **1980**, *19*, 3655–3663.
 (62) Ito, M.; Amagai, H.; Fukui, H.; Kitajima, N.; Moro-oka, Y. *Bull. Chem. Soc. Jpn.* **1996**, *69*, 1937–1945.

Table 4. Resonance Raman Data for Iron(III) Phenolate Products^a

compound	raman shift (cm ⁻¹)											
1 + ¹⁶ O ₂	621	861	961	1001	1254	1273	1298	1451	1480	1559	1598	1606
1 + ¹⁸ O ₂	605	844	942	1001	1245	1273	1294	1451	1480	1559	1598	1606
2 + ¹⁶ O ₂	621	860	963	1001	1254	1274	1301	1452	1481	1559	1599	1604
3 + ¹⁶ O ₂	622	861	965	1001	1254	1275	1302	1453	1482	1560	1600	1607
4 + ¹⁶ O ₂	621	859	961	1001	1252	1273	1299	1452	1482	1560	1600	1606
5 + ¹⁶ O ₂	621	861	961	1001	1253	1275	1300	1453	1482	1560	1599	1607
5 + ¹⁸ O ₂	605	844	961	1001	1244	1273	1297	1451	1481	1560	1599	1607

^a Numbers in bold denote modes sensitive to ¹⁸O substitution.

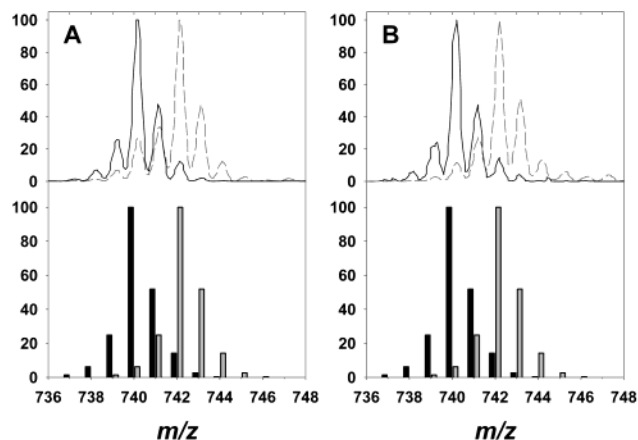


Figure 8. ESI-MS of the molecular ion corresponding to [Fe^{III}(Tp^{Ph2*})]⁺. (A) **1** + ¹⁶O₂ (—) and **1** + ¹⁸O₂ (---) and (B) **5** + ¹⁶O₂ (—) and **5** + ¹⁸O₂ (---). The theoretical distributions for these molecular ions are shown as bar graphs below the isotope splitting observed (¹⁶O black bars, ¹⁸O gray bars).

CR)] affords the resonance Raman spectrum shown in Figure 9A (Table 4), which contains features expected for an iron(III)-phenolate complex.^{63–65} Characteristic peaks are observed in the 1200–1600 cm⁻¹ region arising from ring deformation modes.⁶⁴ Two features at 1254 and 1298 cm⁻¹ downshift in the ¹⁸O isotopomer derived from the reaction of **1** with ¹⁸O₂ and thus can be associated with aromatic ring modes with some C–O stretching character. The peak at 621 cm⁻¹ is also sensitive to isotopic substitution, downshifting 16 cm⁻¹ upon introduction of ¹⁸O (Figure 9B), and can be assigned as the ν(Fe–OAr) mode.⁶³

The phenolate-to-iron(III) charge-transfer transition also provides a convenient spectroscopic probe for monitoring product formation. Complexes **1**–**3** react with dioxygen over the course of 60 min and develop the intense bands at 650 nm associated with [Fe(Tp^{Ph2*})(O₂CR)] (Figure 6). The yields of [Fe(Tp^{Ph2*})(O₂CR)] are estimated to be 70, 55, and 60%, respectively, on the basis of the extinction coefficient culled from the crystalline iron(III) phenolate complex, **6**. Analysis of the [Fe(Tp^{Ph2*})(O₂CR)] product obtained from the reaction of **1** and ¹⁸O₂ (98%) shows that ¹⁸O is incorporated into the phenolate—76% based on the ESI mass spectral analysis and 85% based on fitting the ν(Fe–OAr) vibration in the resonance Raman spectrum (Figures 8A and 9). Experiments carried out in the presence of H₂¹⁸O under ¹⁶O₂ atmosphere show no incorporation of label. Analysis of the benzoate generated from

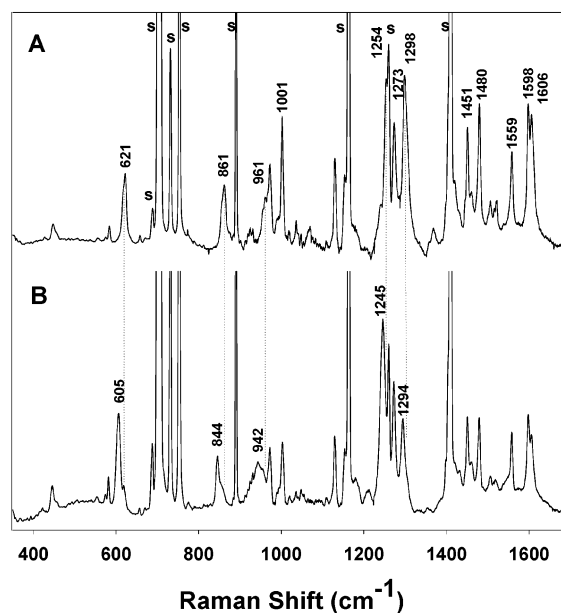


Figure 9. Resonance Raman spectra of the oxygenation products dissolved in CH₂Cl₂: (A) **1** + ¹⁶O₂ and (B) **1** + ¹⁸O₂. All spectra were obtained at 77 K using a backscattering geometry with an excitation wavelength of 632.8 nm. Solvent bands are labeled with an s in panel A. Only peaks sensitive to ¹⁸O substitution are labeled in panel B.

oxidative decarboxylation of the coordinated benzoylformate shows the incorporation of approximately 80% oxygen from ¹⁸O₂ (Figure S6). Thus, one atom of dioxygen is incorporated into the hydroxylated ligand while the other can be found in the carboxylate byproduct. The reaction of **1** with O₂ thus serves as an excellent model for the dioxygenase reactivity observed in the enzymatic systems (Scheme 2).

[Fe(Tp^{Ph2})(BF)] is an excellent candidate for kinetic examination as both the iron(II) precursor and the iron(III) phenolate product have been fully characterized. Detailed kinetic studies on the reaction of **1** and O₂ in benzene establish the bimolecular nature of the oxidation. The appearance of the iron(III) phenolate chromophore can be easily followed at 650 nm, a wavelength with a minimal contribution from the iron(II) precursor. Simple pseudo-first-order kinetic traces are observed and can be fit using the integral method over seven half-lives (Figure 10 (top)). The data can also be fit to a single exponential with mean standard deviations of less than 2% over five to seven half-lives. The benzoylformate complex exhibits a pseudo-first-order rate constant (*k*_{obs}) of 1.0 × 10⁻³ s⁻¹ at 30 °C in an oxygen-saturated solution. This corresponds to a half-life of 670 s or approximately 11 min. While the initial rate of formation of the product at 30 °C depends on the initial concentration of **1**, the pseudo-first-order rate constant exhibits no systematic variation upon changing the concentration of **1** by almost 1 order of

(63) Pyrz, J. W.; Roe, A. L.; Stern, L. J.; Que, L., Jr. *J. Am. Chem. Soc.* **1985**, *107*, 614–620.

(64) Que, L., Jr. in *Biological Applications of Raman Spectroscopy*; Spiro, T. G., Ed.; Wiley: New York, 1988; Vol. 3, pp 491–521.

(65) Carrano, C. J.; Carrano, M. W.; Sharma, K.; Backes, G.; Sanders-Loehr, J. *Inorg. Chem.* **1990**, *29*, 1865–1870.

Table 5. Activation Parameters for Reaction of **1** and Similar Compounds with Dioxygen

compound	temp. range (°C)	ΔH^\ddagger (kJ/mol)	ΔS^\ddagger (J/mol K)	ΔG^\ddagger_{313} (kJ/mol)	ref
1	+10 to +70	25(2)	-179(6)	81(2)	this paper
FeMb (horse)	25	23	-30	32	66
Co(SalMeDPT)	-70 to +25	13(1)	-79	37(1)	67
Hr	+5 to +25	0.6(2)	-58(2)	19(2)	68
MMOH	+3 to +35	92(17)	88(42)	120(17)	69
$\Delta 9D$	+6 to +24	22	-134	64	70
$[\text{Fe}_2(\text{BIPhMe})_2(\text{O}_2\text{CH})_4]$	-35 to +40	33(2)	-39(9)	45(2)	71
$[\text{Fe}_2(\mu\text{-OH})_2(6\text{-Me}_3\text{-TPA})_2]^{2+}$	-80 to -40	17(2)	-175(20)	72(2)	72
$[\text{Fe}_2(\text{HPTP})(\text{OBz})]^{2+}$	-70 to -20	16.5(4)	-114(2)	51.7(4)	73
$[\text{Fe}_2(\text{EtHPTB})(\text{OBz})]^{2+}$	-75 to -10	15.4(6)	-121(3)	53.3(6)	73
$[\text{Fe}_2(\text{HPTMP})(\text{OBz})]^{2+}$	-45 to +20	42(2)	-63(6)	62(2)	73

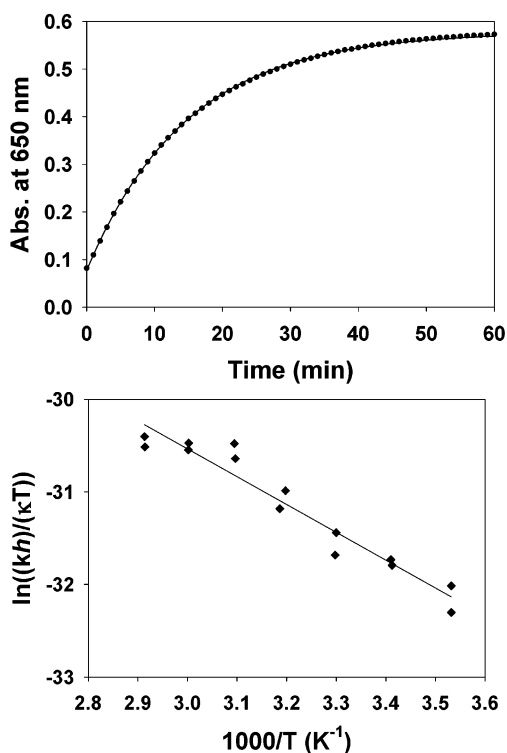


Figure 10. Top: Representative kinetic trace of the reaction between $[\text{FeTp}^{\text{Ph}_2}(\text{BF})]$ and O_2 in benzene. The experimental points are superimposed on the single-exponential fit. Conditions: $T = 30.1(1)^\circ\text{C}$, $[\mathbf{1}]_0 = 0.514\text{ mM}$, and $[\text{O}_2]_0 = 9.2\text{ mM}$. Bottom: Eyring analysis for the reaction of **1** with excess O_2 in benzene between 10 and 70°C , $[\mathbf{1}]_0 = 0.514\text{ mM}$. Experimental data are provided in Table S2 (Supporting Information).

magnitude ($[\mathbf{1}]_0 = 0.1\text{--}0.9\text{ mM}$, Figure S7). Thus, the reaction is clearly first order in iron(II) complex **1**. The order of the reaction with respect to O_2 has also been investigated. A plot of the initial rate absorbance change upon oxygenation versus the initial concentration of O_2 is a straight line (Figure S7). This result demonstrates that the reaction is first order in dioxygen and suggests the reaction is practically irreversible. Therefore, the experimental rate law is second order overall, the rate constant (k_2) being $0.11\text{ M}^{-1}\text{ s}^{-1}$ at 30°C .

$$-\frac{d}{dt}[\mathbf{1}] = -\frac{d}{dt}[\text{O}_2] = \frac{d}{dt}[\text{Fe}(\text{Tp}^{\text{Ph}_2*})(\text{OBz})] = k_{\text{obs}}[\mathbf{1}] = k_2[\mathbf{1}][\text{O}_2] \quad (2)$$

Kinetic data were collected over a 60° temperature range to determine the activation parameters for the reaction of **1** with O_2 . At no point in the course of the reaction was an intermediate observed by optical spectroscopy. Figure 10 (bottom) shows an Eyring analysis of the second-order rate constants. The

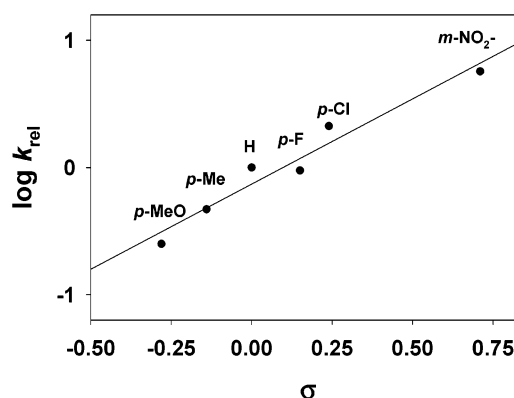
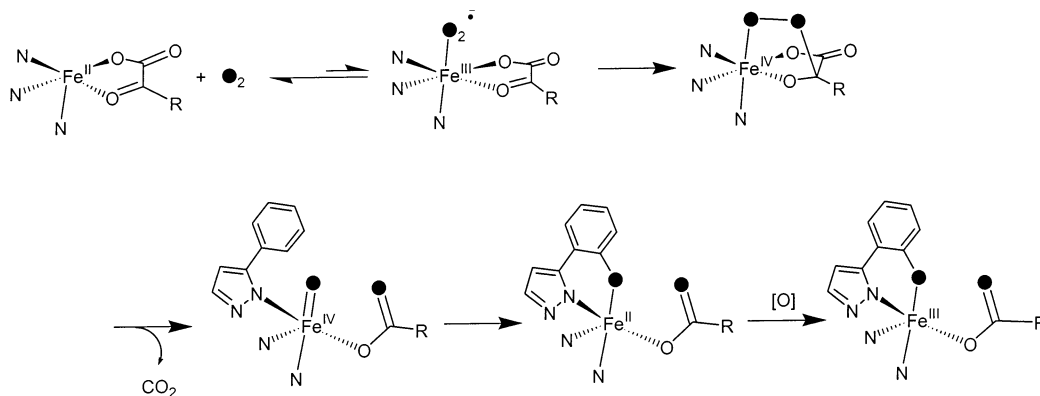


Figure 11. Hammett correlation plot for the oxygenation of $0.5\text{ mM } \mathbf{1}\text{-X}$ in benzene at 30°C ($R^2 = 0.95$, $\rho = 1.3$).

derived activation parameters are listed in Table 5 along with values for other model complexes and oxygen activating enzymes.^{66–73} The enthalpy is in the range of that typically observed for oxygen binding. The large negative entropy of activation suggests that the rate determining step is associative in nature and may also reflect a large entropic cost for reorganization of the nonpolar solvent about a charge-separated intermediate (such as $\text{Fe}^{\text{III}}\text{-O}_2^{\cdot-}$). It is believed that these are composite values, containing contributions from several elementary reactions, and care must be exercised in their interpretation.

The aromatic framework of the benzoylformate ligand allows the introduction of ring substituents that systematically affect the electronic properties of the iron(II) precursors as demonstrated above. These substituted compounds have also been examined under pseudo-first-order conditions with excess oxygen at 30°C . The nature of the phenyl substituent affects the rate of aryl hydroxylation with half-lives ranging from 2 min (**1-NO₂**) to a little more than an hour (**1-OMe**). The reaction rate increases with electron-withdrawing groups, while electron-releasing substituents slow the rate of reaction. A good correlation is obtained between the relative rates and the Hammett parameter σ ($R^2 = 0.95$; σ^+ gives poorer fits). The Hammett plot has a positive slope indicative of a nucleophilic rate-determining step ($\rho = 1.3$, Figure 11). This suggests that withdrawal of electron density from the α -keto carbon accelerates the formation of the iron(III) phenolate product.

Complexes **4** and **5** also react with O_2 under the same conditions to afford 55(5)% of the hydroxylated product; $^{18}\text{O}_2$ labeling experiments with **5** show 90% of the label is incorporated into the product (Figure 8B). Significantly, the reactions of **4** and **5** with O_2 require 2–3 days for completion, almost 2 orders of magnitude slower than the corresponding reactions

Scheme 3. Proposed Mechanism for Hydroxylation of Phenyl Ring with α -Keto Acid Precursor

of **1**–**3** at the same concentrations of iron(II) complex. Interestingly, the time course for the formation of **6** from **5** is more complex than the easily analyzed exponential increase observed for **1** (Figure 10). The carboxylate compounds exhibit a lag phase that makes further detailed kinetic analysis necessary. Nonetheless, it is clear from the above observations that the presence of an α -keto acid in the iron coordination sphere significantly enhances its ability to react with O₂.

Mechanistic Implications. Iron(II)- α -keto carboxylate complexes have previously been shown to activate dioxygen and model the oxidative decarboxylation of α -keto acids carried out by the enzymatic systems.^{27,28,31} The ancillary ligand in these iron(II)- α -keto carboxylate complexes exerts a dramatic effect on the reactivity of the complexes toward O₂, increasing in the order 6-Me₃-TPA, TPA, Tp^{Ph2}, and Tp^{Me2}. The tetradentate 6-Me₃-TPA and TPA ligands afford six-coordinate complexes that react over a period of days,²⁷ while the tridentate Tp^{Ph2} and Tp^{Me2} ligands afford five-coordinate complexes that react within an hour.^{28,30} The difference of nearly 2 orders of magnitude in reaction rate strongly suggests that the coordinative unsaturation of the iron(II) center in the Tp^{R2} complexes and the consequent availability of an O₂ coordination site are important in promoting the oxidative decarboxylation of the bound α -keto acid. This mechanistic principle has also been invoked in explaining the much higher reactivity of the five-coordinate enzyme- α -KG complex in the presence of the primary substrate relative to the six-coordinate complex in the absence of the primary substrate.^{24,74,75}

For the five-coordinate α -keto carboxylate model compounds, we propose the following mechanism for ligand hydroxylation (Scheme 3), which is based on previously proposed mechanisms

for α -keto acid-dependent iron enzymes.^{22–25} O₂ binding to the iron(II) center is postulated to form a reversible adduct, yet unobserved, that can be described as an iron(III)-superoxo species. The large activation entropy is consistent with an associative rate-limiting step. Similarly, large activation enthalpies have been observed for metal complexes that bind O₂ (Table 5).⁷⁶ Once formed, the bound superoxide, which is nucleophilic in character,⁷⁷ can be trapped by the electrophilic α -keto functionality of the bound α -keto acid. The potency of superoxide to bring about cleavage of α -keto acids^{78,79} and the positive ρ value obtained in the Hammett analysis of the [Fe-(Tp^{Ph2})(X-BF)] and [Fe(6-Me₃-TPA)(X-BF)]⁺ complexes²⁷ support such a nucleophilic step, as does the demonstrated increased susceptibility of the α -keto group to exchange with water upon coordination to the iron(II) center.³⁶ Attack at the α -keto carbon affords an iron-peroxo adduct that either directly hydroxylates the phenyl group or undergoes O–O bond cleavage and decarboxylation to generate an iron(IV)-oxo species that carries out the oxidation. The resultant iron(II) phenolate product is then rapidly oxidized by excess oxygen to the green iron(III) phenolate complex observed. The absence of ¹⁸O incorporation when the reaction of **1** and O₂ is carried out in the presence of H₂¹⁸O does not allow us to choose between one of the two possible oxidants. If an iron(IV)-oxo species is involved, as has been proposed for the enzymatic reactions, its lifetime must be too short relative to H₂¹⁸O exchange in the biomimetic transformation.

The key role of the α -keto acid is highlighted by the observations on the corresponding carboxylate complexes. Although the carboxylate compounds can carry out the same O₂-dependent arene hydroxylation of the Tp^{Ph2} ligand, this functionalization at the same concentration of complex (0.5 mM) occurs only at a drastically reduced rate, nearly 2 orders of magnitude slower. Since both types of complexes have Fe^{III}/Fe^{II} potentials around 1 V versus SCE, O₂ adduct formation is thermodynamically unfavorable for either type of complex (assuming that the O₂/O₂^{-•} couple of –630 mV versus NHE⁸⁰ in acetonitrile does not change significantly in benzene). The proximity of the α -keto functionality provides an efficient means

(66) Antonini, E.; Brunori, M. *Hemoglobin and Myoglobin in Their Reactions with Ligands*; North-Holland: Amsterdam, 1971.

(67) Rybak-Akimova, E. V.; Otto, W.; Deardorf, P.; Roesner, R.; Busch, D. H. *Inorg. Chem.* **1997**, *36*, 2746–2753.

(68) Lloyd, C. R.; Eyring, E. M.; Ellis, W. R., Jr. *J. Am. Chem. Soc.* **1995**, *117*, 11993–11994.

(69) Valentine, A. M.; Stahl, S. S.; Lippard, S. J. *J. Am. Chem. Soc.* **1999**, *121*, 3876–3887.

(70) Broadwater, J. A.; Achim, C.; Munck, E.; Fox, B. G. *Biochemistry* **1999**, *38*, 12197–12204.

(71) Feig, A. L.; Masschelein, A.; Bakac, A.; Lippard, S. J. *J. Am. Chem. Soc.* **1997**, *119*, 334–342.

(72) Kryatov, S.; Rybak-Akimova, E. V.; MacMurdo, V. L.; Que, L., Jr. *Inorg. Chem.* **2001**, *40*, 2220–2228.

(73) Feig, A. L.; Becker, M.; Schinder, S.; van Eldik, R.; Lippard, S. J. *Inorg. Chem.* **1996**, *35*, 2590–2601.

(74) Zhou, J.; Kelly, W. L.; Bachmann, B. O.; Gunsior, M.; Townsend, C. A.; Solomon, E. I. *J. Am. Chem. Soc.* **2001**, *123*, 7388–7398.

(75) Zhou, J.; Gunsior, M.; Bachmann, B. O.; Townsend, C. A.; Solomon, E. I. *J. Am. Chem. Soc.* **1998**, *120*, 13539–13540.

(76) Busch, D. H.; Alcock, N. W. *Chem. Rev.* **1994**, *94*, 585–623.

(77) Sawyer, D. T.; Valentine, J. S. *Acc. Chem. Res.* **1981**, *14*, 393–400.

(78) San Fillipo, J., Jr.; Romano, L. J.; Chern, C.-I.; Valentine, J. S. *J. Org. Chem.* **1976**, *41*, 586–588.

(79) San Fillipo, J., Jr.; Chern, C.-I.; Valentine, J. S. *J. Org. Chem.* **1976**, *41*, 1077–1078.

(80) Sawyer, D. T. in *Oxygen Complexes and Oxygen Activation by Transition Metals*; Martell, A. E., Sawyer, D. T., Eds.; Plenum Press: New York, 1988; pp 129–148.

for trapping the nascent superoxide in the cases of **1-3** to drive the overall reaction to completion. For **4** and **5**, the absence of the α -keto moiety would require a different superoxide trapping mechanism that may relate to the formation of a (μ -1,2-peroxo)-diiron(III) adduct like that observed for $[\text{Fe}(\text{Tp}^{\text{IPr}2})(\text{O}_2\text{CR})]$ complexes.^{42,81} Mechanistic details for the latter reaction have not been established and will be the focus of a subsequent publication. Nevertheless, these results emphasize the versatility of a nonheme iron center to activate dioxygen.

An important feature of the α -keto carboxylate complexes described here is the effective coupling between the oxidative decarboxylation of the α -keto acid part of the reaction, which provides the electrons needed for oxygen activation, and the hydroxylation of the phenyl group. In the best case, about 0.7 equiv of phenol is formed per α -keto acid decarboxylated. The degree of coupling is much less efficient for other nonheme iron model systems that mimic enzymatic hydroxylation of arenes using molecular oxygen and a sacrificial electron donor.⁸²⁻⁸⁷ A large excess of reducing agent such as mercaptoethanol, zinc and acetic acid, diphenylhydrazine, hydroquinone, or ascorbate is typically required, making it difficult to determine the ratio of substrate oxidized to reductant used in these systems. Invariably, the oxidizing species formed in such reactions can also oxidize the excess reducing agent instead of the intended substrate. Enzymes avoid this pitfall by compartmentalizing the reducing and oxidizing half reactions. The use of the α -keto acid cofactor is a convenient strategy to control the flow of electrons and may explain the many and diverse types of α -keto acid-dependent enzymes found in biology.^{2,4-9,24} Yet even in the enzymes, there is evidence for uncoupling of oxidative decarboxylation from substrate functionalization, especially when substrate analogues are used.⁸⁸⁻⁹²

The $\text{Fe}(\text{Tp}^{\text{Ph}2})$ α -keto carboxylate complexes described are the only biomimetic systems demonstrated thus far to capture the dioxygenase aspect of the enzyme reactions. ¹⁸O₂ labeling studies show that the elements of dioxygen are incorporated into the phenol product and the carboxylate derived from the α -keto acid. This is very likely a result of the proximity of the phenyl group, which traps the oxidizing species as it is formed in the course of the oxidative decarboxylation of the bound α -keto acid. Undoubtedly, the same proximity principle applies to prolyl hydroxylase, thymine hydroxylase, and other enzymes that exhibit this dioxygen incorporation pattern (Table 6).⁹³⁻¹⁰³ Furthermore, the lack of significant ¹⁸O incorporation from

labeled water into the product suggests that the oxidant responsible for substrate oxidation is either the iron-peroxo intermediate, which is not capable of exchange with solvent water, or the iron(IV)-oxo species, which is capable of solvent exchange but must react with substrate before solvent exchange can occur (Scheme 3).

However, as illustrated in the bottom half of Table 6,¹⁰⁴⁻¹⁰⁷ other α -keto acid-dependent iron enzymes catalyze reactions to afford oxidized substrates with varying degrees of solvent incorporation. The substrate oxidation mechanism in these enzymes must thus involve a species capable of solvent exchange, for example, an iron(IV)-oxo species. Although this high valent species has been proposed in the mechanisms of many nonheme iron enzymes, it has not yet been directly observed in enzymes. However, the first biomimetic nonheme iron(IV)-oxo complexes have just been characterized,^{108,109} which will allow the spectroscopic signatures of the iron(IV)-oxo unit to be established and its reactivity properties to be compared with those of the enzymes.

Last, the aryl hydroxylation in the reaction of $[\text{Fe}(\text{Tp}^{\text{Ph}2})\text{(BF)}]$ and O₂ to produce a phenolate product that then gives rise to a visible chromophore resembles the recently reported self-hydroxylation of $[\text{Fe}(\text{TfdA})(\alpha\text{-KG})]$ and $[\text{Fe}(\text{TauD})(\alpha\text{-KG})]$ complexes. These enzymatic complexes react with O₂ in the absence of the primary substrate, whereby the nearby Trp112 and Tyr73 residues in the respective enzyme active sites are hydroxylated to form a blue or green-brown chromophore.^{106,107} The latter observation demonstrates that, despite the absence of the primary substrate, the enzyme- α -KG complex is still able to activate O₂, albeit slowly, to form an oxidizing species capable of arene hydroxylation. However, the self-hydroxylations of TfdA and TauD differ from the biomimetic reaction in one important respect. The oxygen atom of the hydroxylated tryptophan or the hydroxylated tyrosine derives not from O₂ but from H₂O (Scheme 4), so solvent exchange occurs prior to

(81) Kim, K.; Lippard, S. J. *J. Am. Chem. Soc.* **1996**, *118*, 4914-4915.

(82) Tabushi, I.; Nakajima, T.; Seto, K. *Tetrahedron Lett.* **1980**, *21*, 2565-2568.

(83) Vincent, J. B.; Huffman, J. C.; Christou, G.; Li, Q.; Nanny, M. A.; Hendrickson, D. N.; Fong, R. H.; Fish, R. H. *J. Am. Chem. Soc.* **1988**, *110*, 6898-6900.

(84) Kitajima, N.; Ito, M.; Fukui, H.; Moro-oka, Y. *J. Chem. Soc., Chem. Commun.* **1991**, 102-104.

(85) Hage, J. P.; Sawyer, D. T. *J. Am. Chem. Soc.* **1995**, *117*, 5617-5621.

(86) Funabiki, T.; Yokomizo, T.; Suzuki, S.; Yoshida, S. *Chem. Commun.* **1997**, 151-152.

(87) Ménage, S.; Galey, J.-B.; Dumats, J.; Hussler, G.; Seité, M.; Luneau, I. G.; Chottard, G.; Fontecave, M. *J. Am. Chem. Soc.* **1998**, *120*, 13370-13382.

(88) Tuderman, L.; Myllylä, R.; Kivirikko, K. I. *Eur. J. Biochem.* **1977**, *80*, 341-348.

(89) Puistola, U.; Turpeenniemi-Hujanen, T. M.; Myllylä, R.; Kivirikko, K. I. *Biochim. Biophys. Acta* **1980**, *611*, 51-60.

(90) Holme, E.; Lindstedt, S.; Nordin, I. *Biochem. Biophys. Res. Commun.* **1982**, *107*, 518-524.

(91) Wehbie, R. S.; Punekar, N. S.; Lardy, H. A. *Biochemistry* **1988**, *27*, 2222-2228.

(92) Myllylä, R.; Majamaa, K.; Günzler, V.; Hanauske-Abel, H. M.; Kivirikko, K. I. *J. Biol. Chem.* **1984**, *259*, 5403-5405.

(93) Holme, E.; Lindstedt, G.; Lindstedt, S.; Toft, M. *J. Biol. Chem.* **1971**, *246*, 3314-3319.

(94) Thornburg, L. D.; Lai, M.-T.; Wishnok, J. S.; Stubbe, J. *Biochemistry* **1993**, *32*, 14023-14033.

(95) Kikuchi, Y.; Suzuki, Y.; Tamiya, N. *Biochem. J.* **1983**, *213*, 507-512.

(96) Wu, M.; Begley, T. P.; Myllyharju, J.; Kivirikko, K. I. *Bioorg. Chem.* **2000**, *28*, 261-265.

(97) McNeill, L. A.; Hewitson, K. S.; Gleadle, J. M.; Horsfall, L. E.; Oldham, N. J.; Maxwell, P. H.; Pugh, C. W.; Ratcliffe, P. J.; Schofield, C. J. *Bioorg. Med. Chem. Lett.* **2002**, *12*, 1547-1550.

(98) Hewitson, K. S.; McNeill, L. A.; Riordan, M. V.; Tian, Y.-M.; Bullock, A. N.; Welford, R. W.; Elkins, J. M.; Oldham, N. J.; Bhattacharya, S.; Gleadle, J. M.; Ratcliffe, P. J.; Pugh, C. W.; Schofield, C. J. *J. Biol. Chem.* **2002**, *277*, 26351-26355.

(99) Lloyd, M. D.; Merritt, K. D.; Lee, V.; Sewell, T. J.; Wha-Son, B.; Baldwin, J. E.; Schofield, C. J. *Tetrahedron* **1999**, *55*, 10201-10220.

(100) Baldwin, J. E.; Adlington, R. M.; Schofield, C. J.; Sobey, W. J.; Wood, M. E. *J. Chem. Soc., Chem. Commun.* **1989**, 1012-1015.

(101) Baldwin, J. E.; Adlington, R. M.; Crouch, N. P.; Pereira, I. A. C.; Aplin, R. T.; Robinson, C. *J. Chem. Soc., Chem. Commun.* **1993**, 105-108.

(102) Baldwin, J. E.; Adlington, R. M.; Crouch, N. P.; Pereira, I. A. C. *Tetrahedron* **1993**, *49*, 7499-7518.

(103) Lindblad, B.; Lindstedt, G.; Toft, M.; Lindstedt, S. *J. Am. Chem. Soc.* **1969**, *91*, 4604-4606.

(104) Lindblad, B.; Lindstedt, G.; Lindstedt, S. *J. Am. Chem. Soc.* **1970**, *92*, 7446-7449.

(105) Sabourin, P. J.; Bieber, L. L. *J. Biol. Chem.* **1982**, *257*, 7468-7471.

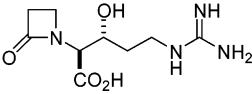
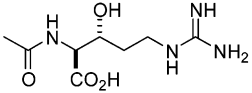
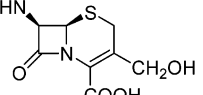
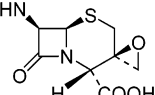
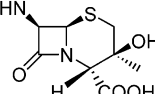
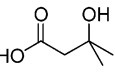
(106) Liu, A.; Ho, R. Y. N.; Que, L., Jr.; Ryle, M. J.; Phinney, B. S.; Hausinger, R. P. *J. Am. Chem. Soc.* **2001**, *123*, 5126-5127.

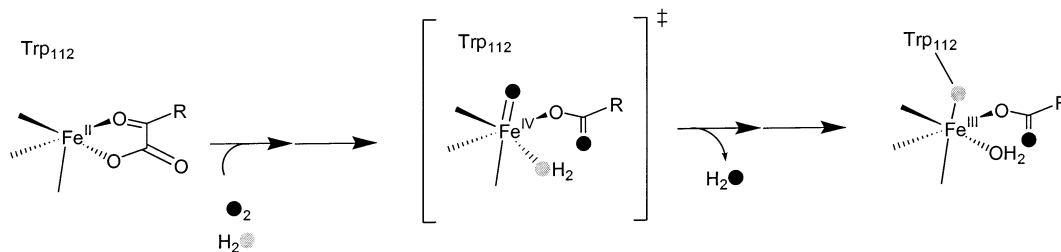
(107) Ryle, M. J.; Liu, A.; Muthukumar, R. B.; Ho, R. Y. N.; Koehntop, K. D.; McCracken, J.; Que, L., Jr.; Hausinger, R. P. *Biochemistry* **2003**, *42*, 1854-1862.

(108) Rohde, J.-U.; In, J.-H.; Lim, M. H.; Brennessel, W. W.; Bukowski, M. R.; Stubna, A.; Münck, E.; Nam, W.; Que, L., Jr. *Science* **2003**, *299*, 1037-1039.

(109) Lim, M. H.; Rohde, J.-U.; Stubna, A.; Bukowski, M. R.; Costas, M.; Ho, R. Y. N.; Münck, E.; Nam, W.; Que, L., Jr. *Proc. Natl. Acad. Sci.* **2003**, *100*, 3665-3670.

Table 6. Oxygen Incorporation by α -Keto Acid-Dependent Enzymes

Enzyme	Functionalized substrate (SO)	¹⁸ O ₂ (%)		H ₂ ¹⁸ O (%)		ref.
		RCO ₂ ⁻	SO	SO	SO	
Thymine hydroxylase	5-(hydroxymethyl)uracil	95	91	---	---	93
	5-(1,2-dihydroxyethyl)uracil	97	---	---	---	94
	5-(methylsulfinyl)uracil	97	---	---	---	94
Prolyl-4-hydroxylase	4-hydroxyproline	---	87	---	---	95
	4-hydroxyproline	---	---	0	---	96
HIF prolyl hydroxylase	4-hydroxyproline	---	> 95	0	---	97
HIF Asn hydroxylase	Hydroxyasparagine	---	100	---	---	98
Clavaminate synthase		---	~70	< 6	---	99
		---	~80	< 10	---	99
DAOC/DAC synthase		> 90	50	40	---	100,101
		---	94	17	---	100,101
		---	70	21	---	102
γ -butyrobetaine hydroxylase	D-carnitine	75	---	---	---	103
Lysyl hydroxylase	Hydroxylysine	---	6.5	---	---	95
HPP hydroxylase	Homogentisate	> 95	30	70	---	104
α -keto isocaproate oxygenase		> 92	15	60	---	105
TfdA (self-hydroxylation)	Trp112 residue	---	0	100	---	106
TauD (self-hydroxylation)	Tyr73 residue	---	0	100	---	107

Scheme 4. TfdA Self-Hydroxylation

the C–O bond forming step. A similar labeling result has been found in the formation of the DOPA208 residue from the F208Y mutant of ribonucleotide reductase R2.¹¹⁰ In the latter case, it is postulated that Y208 is first oxidized by one electron to its radical form and then reacts with the solvent-equilibrated iron-

(III)iron(IV) intermediate to form solvent-labeled DOPA208. The self-hydroxylations of TfdA and TauD may follow an analogous sequence of steps.^{106,107}

(110) Ling, J.; Sahlin, M.; Sjöberg, B.-M.; Loehr, T. M.; Sanders-Loehr, J. *J. Biol. Chem.* **1994**, *269*, 5595–5601.

The Fe(Tp^{Ph2}) model system described in this paper thus serves as an excellent functional model for the α -keto acid-dependent iron enzymes, mimicking many of the features associated with the reaction of enzyme- α -KG complexes with O₂. Our results particularly emphasize the key role the α -keto acid plays in oxygen activation by trapping the initial O₂ adduct and channeling it down the pathway towards O-O bond cleavage. Continued work on this unique family of biomimetic complexes should provide further mechanistic insight into this fascinating and versatile iron(II) α -keto carboxylate center for oxygen activation in biology.

Acknowledgment. This work was supported at the University of Minnesota by the National Institutes of Health (Grant GM-33162 to L.Q., Postdoctoral Fellowship GM-18639 to E.L.H., and Predoctoral Traineeship GM-08700 to M.P.M.) and at the University of Tsukuba by grants from the Japan Society for the Promotion of Science (Nos. 13555257 and 14350471), Kawaski Steel 21st Century Foundation, and the Asahi Glass Foundation. We thank Dr. Victor G. Young, Jr. and William W. Brennessel of the University of Minnesota X-ray Crystal-

lographic Laboratory for determining the crystal structures of **2** and **4–6**. K.F. acknowledges Dr. Frank Neese and Prof. Edward I. Solomon (Stanford University) for preliminary resonance Raman studies of the oxygenated products and Prof. Ken-ichi Okamoto (University of Tsukuba) for his encouragement.

Supporting Information Available: Crystallographic data for **2** and **4–6** (CIF format); structural tables for both independent molecules in unit cell of **2** (Table S1); ¹H NMR parameters (Table S2); Kinetic Data for Eyring Analysis (Table S3); Correlation of LMCT with Hammett σ (Figure S1); ¹H NMR spectra of **2**, **3**, and **5** (Figure S2); COSY spectrum of **4** (Figure S3); CV of **1-NO₂**, **1**, and **1-OMe** and correlation with Hammett σ (Figure S4); EPR spectra of oxygenated products for **1** + O₂ (Figure S5); Low Resolution MS of PhCO¹⁸OMe (Figure S6); and determination of order in **1** and O₂ (Figure S7) (PDF format). This material is available free of charge via the Internet at <http://pubs.acs.org>.

JA028867F